THE ASTROPHYSICAL JOURNAL, 399:462–477, 1992 November 10

DYNAMICALLY HOT GALAXIES. I. STRUCTURAL PROPERTIES[1]

RALF BENDER[2]
Landessternwarte Königstuhl, D6900 Heidelberg, Germany
DAVID BURSTEIN
Department of Physics and Astronomy, Arizona State University, Tempe, AZ 85287-1504
AND
S. M. FABER
UCO/Lick Observatory, University of California, Santa Cruz, CA 95064
Received 1992 February 7; accepted 1992 May 18

ABSTRACT

The structural properties of dynamically hot galaxies are analyzed by combining central velocity dispersion, effective surface brightness, and effective radius into a new 3-space (κ), in which the axes are parameters that are physically meaningful. The degree of velocity dispersion anisotropy is also used. Hot galaxies are found to divide into groups in κ-space that closely parallel conventional morphological classifications: luminous ellipticals, compacts, bulges, bright dwarfs, and dwarf spheroidals. Most systems lie close to the fundamental plane defined by luminous Virgo and Coma ellipticals, indicating similar M/L. However, bulges have somewhat low apparent M/L, while dwarfs have slightly high M/L. The extreme M/L excess of some dwarf spheroidals sets them apart from all other dynamically hot galaxies and indicates strong domination by dark matter.

A major sequence is defined by luminous ellipticals, bulges, and most compacts, which together constitute a smooth continuum in κ-space. Several properties vary smoothly with mass along this continuum, including bulge-to-disk ratio, radio properties, rotation, degree of velocity anisotropy, and "unrelaxed." or peculiar, kinematics. These trends are consistent with the idea that the final mergers leading to larger galaxies in this group were systematically more stellar (and less gaseous) than those in smaller galaxies (i.e., a "gas/stellar," or GS, continuum). Structural parameters along this continuum are compared to those predicted for cold dark matter (CDM) in κ-space. CDM predictions can be made to fit the data only if dissipation *decreases* significantly with increasing mass. This conclusion is consistent with a declining role for gas versus stars with increasing mass as implied by the GS continuum.

A second major sequence is comprised of dwarf ellipticals and dwarf spheroidals. These systems populate an elongated locus running at right angles to the main elliptical locus. Various evidence suggests that mass loss is a major factor in hot dwarf galaxies, but the dwarf sequence cannot be simply a mass-loss sequence as it has the wrong direction in κ-space. Hot dwarfs must have come from a range of progenitor galaxies that are not visible today as hot galaxies. The existence of a primarily one-dimensional hot dwarf sequence is surprising and may be at least partially an artifact of selection effects.

The most massive and the least massive hot galaxies are anisotropic, separated by a strip of galaxies of intermediate mass that are isotropic rotators. The origin of anisotropy in giants and dwarfs is probably different, with that of giants likely being due to stellar mergers, and that in dwarfs possibly being due to expansion following mass loss, or a low rate of internal cloud-cloud collisions due to small collapse factors.

Subject headings: galaxies: elliptical and lenticular, cD — galaxies: kinematics and dynamics — galaxies: photometry

1. INTRODUCTION

The amount of detailed information on the internal kinematics and structure of dynamically hot galaxies has grown enormously over the past 5 yr.

1. A "fundamental plane" exists for the physical properties of elliptical galaxies in the three-dimensional space defined by central velocity dispersion (σ_0), effective surface brightness (SB_e), and effective radius (r_e) (Dressler et al. 1987; Djorgovski & Davis 1987; Faber et al. 1987). Although the universality of this fundamental plane is still a matter of debate with regard to slope and zero point (cf. Lucey, Bower, & Ellis 1991 and below), its existence is not in question.

2. Ellipticals and bulges (of spirals and S0's) form a single continuous sequence in diagrams of structural properties (e.g., Kormendy 1985; Binggeli & Cameron 1991). This sequence appears distinct from that defined by dwarf ellipticals *and* dwarf irregulars (Kormendy 1985, 1987; Binggeli & Cameron 1991; see, however, Sandage, Binggeli, & Tammann 1985; Nieto 1988).

3. Bulges and faint ellipticals differ from luminous ellipticals with regard to rotation and isotropy of velocity dispersions (Kormendy & Illingworth 1982; Davies et al. 1983, hereafter DEFIS). Bulges and faint ellipticals are generally isotropic and rotationally flattened, while luminous ellipticals rotate less and are flattened by an anisotropic velocity dispersion.

4. *Diffuse* dwarf ellipticals have anisotropic dynamics similar to those of bright elliptical galaxies, while most

[1] This paper is dedicated to the memory of Jean-Luc Nieto, who died suddenly and tragically in an accident on 1992 January 5. He will be warmly remembered as an enthusiastic and energetic astronomer by his many friends, and his friendly smile will be missed.

[2] Visiting Astronomer of the German-Spanish Astronomical Observatory, Calar Alto.

compact ellipticals are rotationally flattened (Bender & Nieto 1990, hereafter BN90; Bender, Paquet, & Nieto 1991).

5. Many ellipticals show evidence of dynamically distinct substructures: kinematically decoupled cores (Franx & Illingworth 1988; Jedrzejewski & Schechter 1988; Bender 1988b, 1990); correlated substructure in rotation and line strength profiles (Bender 1992); and a wide variety of optical disturbances, including shells, plumes, jets, twists, and dust (e.g., Schweizer 1990).

6. Metal abundance (as measured by the Mg_2 index) in elliptical galaxies increases with both luminosity and central velocity dispersion (e.g., Burstein et al. 1988b). The relationship with σ_0 is tighter, though it still shows some intrinsic scatter (Burstein et al. 1988b; Bender 1992).

7. The intrinsic scatter of the Mg_2–σ_0 relation for luminous ellipticals is, at least for one sample of galaxies, correlated with the degree of disturbance in the optical appearance of the galaxy (Schweizer et al. 1990).

Along with this explosive growth in observational data has come an increased understanding of the physical processes at work in the formation and evolution of hot stellar systems. Principal among these is the concept of merging or, alternately, hierarchical clustering. Originally suggested by Toomre (1977), merging and clustering are now seen as natural and unavoidable aspects of any bottom-up galaxy formation scenario (e.g., Blumenthal et al. 1984). Many of the original objections to formation of ellipticals by merging (Ostriker 1980; Gunn 1987) can be overcome by recognizing that many mergers are gaseous and involve dissipation and a concomitant increase in phase-space density (Hernquist & Barnes 1991).

Of the points above, (5) and (6) are especially supportive of merging. This view is reinforced by detailed studies of individual systems that are now believed to be in various stages of postmerger coalescence (e.g., NGC 7252, Schweizer 1982, 1990). We argue below that others of these observational points are also consistent with the merger picture.

A second key process operating in hot stellar systems, especially among low-luminosity galaxies, is mass loss. Several authors have noted that the low surface brightness of diffuse dwarf Es might be explained in this manner, through either supernova-driven mass loss (Dekel & Silk 1986) or ram-pressure stripping (Faber & Lin 1983; Kormendy 1987). We explore the consequences of mass loss (the precise mechanism does not matter) for both diffuse dwarf ellipticals and more luminous hot stellar systems.

This paper is the first of several that intend to explore the relationships among the physical properties and stellar populations of dynamically hot stellar systems. In the present paper, we concentrate on only the structural properties. We use as our principal investigative tool the fundamental plane described in (i) above. We show that this 3-space, heretofore used only for luminous ellipticals, is also a useful way to compare all dynamically hot galaxies, including luminous ellipticals, compact ellipticals, bulges of S0/Sa galaxies, and dwarf ellipticals. S0/Sa galaxies are preferred for this study, as it is easier to separate bulge properties from disk properties in galaxies with large bulge-to-disk ratios. Although many of our conclusions reinforce previous interpretations, the present treatment is new in considering all known hot galaxy types simultaneously and uniformly, utilizing the full 3-space defined by their properties rather than just two-dimensional projections of those properties. In particular, we trace the effects of merging and mass loss in the full 3-space, which has not been done before.

The data are presented in § 2. In § 3 we derive vectors for the various physical processes that can move galaxies within the 3-space and compare these directions to the orientation of the fundamental plane. The actual distributions of different galaxy types are discussed in § 4 and compared to the vectors for the physical processes. Concluding discussion is given in § 5, together with a summary of outstanding questions.

2. DATA

The sample for this investigation was selected on the basis that (*a*) all galaxies have spatially resolved kinematics (for determining internal rotation and velocity anisotropy), and (*b*) the sample cover all known types of dynamically hot galaxies. A compromise was made for dwarf spheroidals, for which only the Fornax dwarf has spatially resolved kinematics, and for bulges, for which 11 of 19 have no measure of anisotropy. This compromise was necessary in order to have a sufficient number of objects in these categories.

The following data are available for each galaxy: central velocity dispersion (σ_0), effective radius (r_e), mean effective surface brightness SB_e, and absolute magnitude. SB_e and r_e are defined in terms of the half-light radius of the galaxy, and these two parameters, combined with σ_0 defined the fundamental plane for bright ellipticals. All but the above-mentioned galaxies have their degree of velocity anisotropy parametrized by the ratio $(v/\sigma_0)^*$, defined by BN90 as the ratio of observed v/σ_0 to that expected for an oblate isotropic rotating galaxy of that ellipticity. Galaxies are considered to be anisotropic if $(v/\sigma_0)^* < 0.7$ [$\log (v/\sigma_0)^* < -0.15$], following BN90. These data, together with their sources, are given in Table 1.

When available, we used the heliocentric group redshifts given in Faber et al. (1989), or simply individual redshifts. All redshifts were corrected to the centroid of the Local Group using the prescription of Yahil, Tammann, & Sandage (1977), and distances were derived using $H_0 = 50$ km s^{-1} Mpc^{-1}. We have avoided using more detailed models of the Hubble flow (e.g., Faber & Burstein 1988) that were derived from these same ellipticals so as not to narrow the fundamental plane artificially. For Local Group objects distances are based on color magnitude diagrams and were taken from various sources (listed in Table 1). The central velocity dispersions (σ_0) for giant ellipticals used here compare favorably with those measured by Davies et al. (1987) for galaxies with $\sigma_0 \geq 90$ km s^{-1}. Below that value, the spectral resolution employed by Davies et al. was generally not high enough to recover accurate velocity dispersions.

For clarity, we have divided the sample of dynamically hot galaxies into six separate categories based on morphology and absolute luminosity: 48 giant ellipticals (total blue absolute magnitude, $M_T \leq -20.5$), 20 intermediate ellipticals ($-20.5 < M_T \leq -18.5$), 12 bright dwarf ellipticals ($M_T > -18.5$), four NGC 4486B–type compact ellipticals, 19 bulges of disk galaxies, and five lower luminosity dwarf spheroidals. This classification is straightforward except for the division between bright dwarf ellipticals and compacts, for which specific cases are further discussed in §§ 4.4 and 4.5.

3. THE FUNDAMENTAL PLANE AND PHYSICAL PROCESSES

3.1. *The Fundamental Plane of Elliptical Galaxies*

Among dynamically hot galaxies, giant ellipticals have been the most extensively investigated. Dressler et al. (1987), Faber et al. (1987), and Djorgovski & Davis (1987) showed that these objects lie in a plane in the 3-space defined by σ_0, SB_e, and r_e.

TABLE 1

OBSERVERED PROPERTIES OF DYNAMICALLY HOT GALAXIES

Galaxy (1)	l (2)	b (3)	Type (4)	Distance (5)	S (6)	log σ_0 (7)	Source (8)	log r_e (9)	SB_e (10)	M_T (11)	Source (12)	A_B (13)	log (v/σ_0)* (14)
Giant Ellipticals													
NGC 315	124.6	−32.5	LA	107.2	1	2.546	1	1.486	22.36	−23.61	1	0.26	−1.046
NGC 584	149.8	−67.6	E4	39.6	1	2.337	1	0.724	20.44	−21.72	1	0.13	0.190
NGC 636	155.1	−67.4	E3	39.6	1	2.194	1	0.562	20.71	−20.65	1	0.11	0.017
NGC 720	173.0	−70.4	E5	35.8	2	2.392	1	0.840	21.14	−21.60	1	0.00	−0.638
NGC 777	139.7	−29.2	E1	99.4	1	2.542	1	1.134	21.60	−22.61	1	0.15	−0.558
NGC 821	151.6	−47.6	E6	37.7	2	2.298	1	0.922	21.85	−21.31	1	0.16	−0.155
NGC 1052	182.0	−57.9	E4	29.3	1	2.313	1	0.723	21.11	−21.05	1	0.06	0.000
NGC 1395	216.2	−52.1	E2	31.0	1	2.412	1	0.836	21.22	−21.50	1	0.01	0.041
NGC 1399	236.7	−53.6	E1	26.4	1	2.491	1	0.737	20.68	−21.55	1	0.00	−0.602
NGC 1404	236.9	−53.6	E1	26.4	1	2.353	1	0.537	20.02	−21.21	1	0.00	−0.013
NGC 1407	209.6	−50.4	E0	31.0	1	2.455	1	1.041	21.85	−21.90	1	0.16	−0.076
NGC 1549	265.4	−43.8	E0	19.6	1	2.312	1	0.658	20.96	−20.87	1	0.00	−0.180
NGC 1600	200.4	−33.2	E3	98.6	1	2.506	1	1.360	22.17	−23.17	1	0.08	−1.301
NGC 1700	203.7	−27.6	E4	81.1	1	2.368	1	0.735	19.94	−22.28	1	0.12	−0.097
NGC 2300	127.7	27.8	LA0	45.6	1	2.430	1	0.905	21.51	−21.56	1	0.22	−1.097
NGC 2974	239.5	35.0	E4	34.5	2	2.346	1	0.795	21.28	−21.24	1	0.11	0.188
NGC 3091	268.8	27.5	E3	76.1	1	2.463	1	1.003	21.52	−22.04	1	0.14	−0.420
NGC 3557	281.6	21.1	E3	54.3	2	2.465	1	1.001	21.01	−22.54	1	0.55	0.041
NGC 3607	230.6	66.4	E1	20.4	1	2.394	1	0.816	21.61	−21.02	1	0.00	−0.036
NGC 3610	143.5	54.5	E5	39.1	1	2.201	1	0.388	19.25	−21.23	1	0.00	0.041
NGC 3613	144.3	55.1	E6	39.0	1	2.323	1	0.667	20.78	−21.10	1	0.00	−0.076
NGC 3640	256.9	57.8	E3	27.0	1	2.246	1	0.639	20.82	−20.92	1	0.10	0.170
NGC 3904	287.0	31.7	E2	31.6	1	2.333	1	0.555	20.50	−20.82	1	0.18	−0.444
NGC 4125	130.2	51.3	E6P	38.3	1	2.359	1	1.049	21.46	−22.33	1	0.03	−0.032
NGC 4168	267.7	73.3	E2	43.8	2	2.259	1	0.987	22.23	−21.25	1	0.05	−0.589
NGC 4261	281.8	67.4	E2	41.0	2	2.468	1	0.889	21.25	−21.74	1	0.00	−1.000
NGC 4365	283.8	69.2	E3	20.7	1	2.394	1	0.752	21.42	−20.88	1	0.00	−1.097
NGC 4374	278.2	74.5	E1	20.7	1	2.458	1	0.743	20.81	−21.45	1	0.13	−1.046
NGC 4406	279.1	74.6	E3	20.7	1	2.398	1	0.954	21.65	−21.66	1	0.11	−0.745
NGC 4472	286.9	70.2	E2	20.7	1	2.458	1	1.014	21.40	−22.21	1	0.00	−0.328
NGC 4494	228.6	85.3	E1	22.4	1	2.095	1	0.697	20.97	−21.06	1	0.06	0.093
NGC 4589	124.2	42.9	E2	36.6	1	2.332	1	0.870	21.67	−21.22	1	0.04	−0.244
NGC 4621	294.4	74.4	E5	20.7	1	2.381	1	0.673	20.98	−20.93	1	0.07	−0.092
NGC 4636	297.8	65.5	E0	20.7	1	2.281	1	0.996	22.23	−21.29	1	0.01	−0.602
NGC 4649	295.9	74.3	E2	20.7	1	2.533	1	0.873	21.10	−21.81	1	0.04	−0.337
NGC 4697	301.6	57.1	E6	20.4	2	2.218	1	0.876	21.41	−21.51	1	0.04	−0.108
NGC 4889	57.2	87.9	E4	137.9	1	2.581	1	1.326	21.96	−23.21	1	0.05	−1.320
NGC 5322	110.3	55.5	E3	42.1	1	2.350	1	0.861	20.82	−22.03	1	0.00	−0.585
NGC 5576	348.7	57.9	E3	30.4	1	2.272	1	0.458	20.18	−20.66	1	0.04	−0.658
NGC 5846	0.4	48.8	E0	31.9	1	2.444	1	1.110	22.25	−21.85	1	0.14	−0.986
NGC 6411	89.7	32.6	E2	78.4	2	2.192	1	1.010	21.82	−21.78	1	0.14	−1.301
NGC 6909	352.8	−35.5	E6	56.0	1	2.172	1	0.924	21.84	−21.32	1	0.07	−0.538
NGC 7507	23.4	−68.0	E0	32.1	1	2.377	1	0.692	20.63	−21.38	1	0.20	−0.444
NGC 7619	87.7	−48.3	E2	74.3	1	2.528	1	1.067	21.53	−22.35	1	0.16	−0.276
NGC 7626	87.9	−48.4	E1P	74.3	1	2.369	1	1.137	21.87	−22.36	1	0.16	−0.921
NGC 7785	98.5	−54.3	E5	80.7	2	2.464	1	1.023	21.44	−22.22	1	0.17	−0.328
IC 1459	4.7	−64.1	E3	33.1	1	2.488	1	0.796	20.81	−21.71	1	0.00	−0.658
IC 4296	313.5	28.0	E0	69.2	1	2.509	1	1.286	22.07	−22.90	1	0.12	−0.194
Intermediate Ellipticals													
NGC 1379	236.7	−54.1	E0	27.4	1	2.125	1	0.738	21.79	−20.44	1	0.00	0.056
NGC 1439	215.1	−50.4	E1	31.0	1	2.194	1	0.796	22.15	−20.38	1	0.07	−0.493
NGC 2694	167.3	40.2	E1	89.2	1	2.176	4	0.110	19.70	−19.70	4	0.07	0.044
NGC 3156	238.3	45.1	L	22.7	1	1.845	4	0.744	22.49	−19.77	4	0.04	0.058
NGC 3193	213.0	54.9	E2	23.9	1	2.311	1	0.444	20.69	−20.08	1	0.08	−0.099
NGC 3377	231.2	58.3	E5	13.2	1	2.116	1	0.341	20.76	−19.49	1	0.06	−0.142
NGC 3379	233.5	57.6	E1	13.2	1	2.303	1	0.356	20.16	−20.17	1	0.05	−0.086
NGC 3608	230.4	66.5	LAS0	20.4	1	2.310	1	0.547	21.41	−19.87	1	0.00	−0.353
NGC 3818	273.6	52.7	E5	25.7	2	2.314	1	0.427	21.19	−19.49	1	0.11	−0.031
NGC 4278	193.8	82.8	E1	14.6	1	2.425	1	0.369	20.60	−19.79	1	0.10	−0.150
NGC 4291	125.6	41.6	E2	36.7	1	2.413	1	0.420	20.25	−20.40	1	0.06	−0.284
NGC 4387	278.8	74.5	E5	20.7	1	1.922	1	0.193	20.80	−18.71	1	0.13	−0.156
NGC 4473	281.6	75.4	E5	20.7	1	2.250	1	0.405	20.19	−20.38	1	0.04	−0.398
NGC 4478	283.4	74.4	E2	20.7	1	2.174	1	0.152	19.87	−19.44	1	0.09	−0.024
NGC 4551	288.2	74.7	E3	20.7	1	1.999	1	0.253	20.95	−18.86	1	0.12	−0.257
NGC 4564	289.6	73.9	E6	20.7	1	2.185	1	0.342	20.64	−19.61	1	0.04	0.023
NGC 4660	296.8	74.0	E5	20.7	1	2.296	1	0.112	19.72	−19.39	1	0.00	0.016
NGC 4742	303.1	52.4	E4	22.3	2	1.970	1	0.104	19.36	−19.71	1	0.09	0.209
NGC 5831	359.4	49.0	E3	31.9	1	2.220	1	0.619	21.42	−20.22	1	0.13	−0.732
NGC 5845	0.3	48.9	E3	31.9	1	2.400	1	−0.200	18.38	−19.17	2	0.14	−0.041

TABLE 1—*Continued*

Galaxy (1)	l (2)	b (3)	Type (4)	Distance (5)	S (6)	log σ_0 (7)	Source (8)	log r_e (9)	SB_e (10)	M_T (11)	Source (12)	A_B (13)	log $(v/\sigma_0)^*$ (14)
Bright Dwarf Ellipticals													
NGC 147	119.8	−14.3	dE5	0.7	3	1.369	2	−0.187	23.32	−14.60	3	0.71	−0.409
NGC 185	120.8	−14.5	dE2	0.7	3	1.352	2	−0.237	22.60	−14.80	3	0.78	−1.000
NGC 205	120.7	−21.1	dE5	0.7	3	1.623	2	−0.108	22.32	−15.60	3	0.17	−1.350
NGC 3605	230.6	66.4	E4	20.4	1	2.078	1	0.236	21.42	−18.31	1	0.00	−0.132
NGC 3641	257.0	57.8	E1	27.0	1	2.217	4	0.209	21.32	−18.27	4	0.10	0.185
NGC 4431	281.0	74.1	dS0,N	20.7	1	1.830	5	0.250	22.60	−18.00	5	0.08	0.000
NGC 4467	286.7	70.2	E2	20.7	1	1.826	4	−0.016	21.74	−16.72	4	0.00	−0.289
NGC 4515	280.6	78.3	L	20.7	1	1.954	4	0.170	21.30	−18.49	4	0.03	−0.259
IC 0794	281.8	74.0	dE3,N	20.7	1	1.730	4	0.340	22.92	−17.50	4	0.05	−0.460
IC 3393	282.5	73.9	dE7,N	20.7	1	1.740	5	0.160	22.62	−16.95	5	0.10	−0.300
UGC 7436	272.8	75.9	dE5	20.7	1	1.650	5	0.220	22.90	−16.90	5	0.08	−0.350
V 0351	282.5	66.6	dE7	20.7	1	1.813	4	0.080	22.34	−16.70	4	0.00	−0.637
Compact Ellipticals													
NGC 221	121.2	−22.0	cE2	0.7	3	1.903	3	−0.947	18.33	−15.70	3	0.31	−0.301
NGC 4486B	283.4	74.6	cE0	20.7	1	2.301	4	−0.680	18.30	−17.40	4	0.09	−0.013
NGC 5846A	0.4	48.8	cE2	31.9	1	2.230	4	−0.480	18.20	−18.49	4	0.14	−0.011
IC 0767	268.8	72.2	cE3	20.7	1	1.700	4	−0.280	19.90	−17.40	4	0.03	−0.621
Dwarf Spheroidals													
For	237.3	−65.7	dSph	0.1	4	1.100	6	−0.190	25.60	−12.00	6	0.10	−0.320
Scl	147.2	−85.2	dSph	0.1	4	0.800	7	−0.590	25.10	−10.50	6	0.05	...
Car	260.2	−22.3	dSph	0.1	4	0.790	7	−0.700	26.30	−8.80	6	0.06	...
Dra	86.4	34.7	dSph	0.1	4	1.050	7	−0.820	26.50	−7.90	6	0.07	...
UMi	105.0	44.8	dSph	0.1	4	1.000	7	−0.700	27.20	−7.90	6	0.03	...
Bulges													
NGC 16	111.6	−34.2	LX	67.6	5	2.260	9	0.366	19.59	−20.80	8	0.17	...
NGC 474	136.8	−58.7	LAS0	51.0	5	2.233	9	0.356	20.09	−20.25	8	0.06	...
NGC 936	168.6	−55.3	LBT	30.2	5	2.286	9	0.555	20.41	−20.92	8	0.05	...
NGC 1175	147.7	−14.1	LAR	113.7	5	2.301	8	0.640	20.10	−21.75	7	0.56	−0.130
NGC 1553	265.6	−43.7	LAR0	21.1	5	2.230	10	0.348	19.24	−21.06	7	0.00	−0.036
NGC 2549	159.7	34.2	LAR0	24.1	5	2.146	8	−0.030	18.80	−19.72	7	0.12	0.040
NGC 2639	168.9	38.2	RSAR	65.4	5	2.255	11	0.872	22.02	−20.90	8	0.10	...
NGC 2778	189.2	43.0	LA	39.6	6	2.274	9	0.054	20.69	−18.14	8	0.02	...
NGC 2880	151.5	41.8	LB	32.9	5	2.158	9	0.387	20.60	−19.90	8	0.09	...
NGC 3300	228.5	56.1	LXR0	57.3	5	2.164	11	0.377	21.04	−19.41	8	0.07	...
NGC 3115	247.8	36.8	L	8.7	5	2.342	1	0.189	19.75	−19.70	7	0.10	0.120
NGC 4026	142.0	64.2	L	19.0	5	2.204	8	−0.270	18.20	−19.10	7	0.04	−0.050
NGC 4036	133.0	54.3	L	30.2	5	2.290	9	0.267	20.21	−19.69	8	0.03	...
NGC 4111	149.5	71.7	LAR	16.5	5	2.176	8	−0.480	17.90	−18.33	7	0.00	−0.070
NGC 4169	197.4	81.1	L	76.5	5	2.346	9	0.687	20.76	−21.24	8	0.02	...
NGC 4281	282.8	67.0	L	49.0	5	2.455	9	0.850	21.37	−21.44	8	0.00	...
NGC 4594	298.5	51.2	SAS1	17.5	5	2.342	8	0.910	21.00	−22.51	7	0.12	−0.050
NGC 5380	74.3	72.7	LA	61.2	5	2.199	11	0.030	19.10	−19.61	8	0.00	...
NGC 7332	87.4	−29.7	LP	29.7	5	2.130	8	0.010	18.30	−20.41	7	0.11	−0.110

NOTES.—Col. (1).—Galaxy name according to major catalogs.

Cols. (2), (3).—Galactic longitude l and galactic latitude b, according to de Vaucouleurs et al. (1976; RC2), Sulentic & Tifft (1973; RNGC), and as derived from the celestial coordinates given in Binggeli et al. (1985).

Col. (4).—Type according to RC2 and Binggeli et al. Exceptions are: NGC 147, NGC 185, NGC 205 were reclassified as dE (originally E in RC2); NGC 3641, NGC 4467, VCC 351 were reclassified based on CCD photometry by Prugniel (1989) (originally cE and cE candidates in RC2 and Binggeli et al.); and the type of NGC 2778 taken from Kent (1985).

Col. (5).—Distances in Mpc ($H_0 = 50\ \mathrm{km\ s^{-1}\ Mpc^{-1}}$).

Col. (6).—Sources for distances: 1 = group redshift from Faber et al. (1989) corrected to centroid of Local Group; 2 = individual redshift from Faber et al. (1989) corrected to centroid of Local Group; 3 = Sandage & Tammann (1981); 4 = Zinn (1985); 5 = individual redshift from Sandage & Tammann (1981) corrected to centroid of Local Group; 6 = individual redshift from Davies et al. (1983) corrected to centroid of Local Group.

Col. (7).—Log σ_0, logarithm of central velocity dispersion (σ_0), in units of $\mathrm{km\ s^{-1}}$.

Col. (8).—Sources of values of σ_0: 1 = Davies et al. (1987); 2 = Tonry (1984); 3 = Bender et al. (1991); 4 = Bender & Nieto (1990); 5 = Bender, unpublished; 6 = Mateo et al. (1991); 7 = Freeman (1987); 8 = Seifert (1990); 9 = Whitmore et al. (1985); 10 = Kormendy & Illingworth (1982). 11 = Bender (unpublished).

Col. (9).—Log r_e, logarithm of effective half light radius, r_e, in kpc, for the whole galaxy (ellipticals) and for the bulge only (spirals and S0's). The value for r_e is derived from an $r^{1/4}$ fit to the growth curve, or from an $r^{1/4}$ fit to surface brightness profile as a function of $(ab)^{1/2}$. The value of r_e for dwarf spheroidals is derived from core and tidal radii via King models.

Col. (10).—SB_e, mean surface brightness within effective radius in B band for the whole galaxy (ellipticals) and only for the bulge (spirals and S0's), in B mag $\mathrm{arcsec^{-2}}$.

Col. (11).—M_T, absolute magnitude in B band for the whole galaxy (ellipticals) and only for the bulge (spirals and S0's).

Col. (12).—Sources for r_e, SB_e, and M_T: 1 = Burstein et al. (1987); 2 = Burstein et al. (1987), corrected by unpublished CCD photometry; 3 = RC2 and Kent (1987); 4 = Prugniel (1989); 5 = Binggeli, private communication, and own unpublished CCD photometry; 6 = Freeman (1987) and assuming $B - V = 0.6$ mag; 7 = Seifert (1990); 8 = Kent (1985).

Col. (13).—Galactic extinction, A_B from Burstein & Heiles (1984), and Burstein (unpublished).

Col. (14).—The anisotropy parameter $(v/\sigma_0)^*$, expressed in logarithmic form, derived in accordance with Bender & Nieto (1990). Sources of data are Schechter & Gunn (1978); Kormendy & Illingworth (1982); Davies & Illingworth (1983); Davies et al. (1983); Tonry (1984); Paltoglou & Freeman (1987); Bender (1988a); Davies & Birkinshaw (1988); Franx et al. (1989); Bender & Nieto (1990); Bender et al. (1991); and Bender (unpublished).

The existence of this plane can be thought of as a consequence of the virial theorem, but the precise tilt in 3-space depends on the systematic variation of mass-to-light ratio with luminosity.

The fundamental plane of elliptical galaxies can be derived by means of a principal component analysis. To avoid distance uncertainties, we choose for our fiducial sample only Virgo cluster elliptical galaxies with velocity dispersions larger than 90 km s^{-1} as tabulated by Faber et al. (1989). From this data set we obtain

$$r_e \propto (\sigma_0^2)^{0.7} I_e^{-0.85} , \quad (1)$$

similar to the values quoted by Faber et al. (1987) for several samples of galaxies (with I_e defined as $10^{-0.4(SB_e-27)}$. If σ_0^2 is used instead of σ_0, the observed variance of all three variables is about the same for luminous ellipticals ($\Delta \log \sigma_0^2 \approx \Delta \log I_e \approx \Delta \log r_e \approx 0.4$), so the variables are quasi-normalized.

The fundamental plane of elliptical galaxies can be interpreted in the following way. Using the identities

$$L = c_1 I_e r_e^2 , \quad (2)$$

$$M = c_2 \sigma_0^2 r_e , \quad (3)$$

with L and M representing luminosity and mass and c_1, c_2 being structure constants, we find

$$r_e = (c_2 c_1^{-1})(M/L)^{-1} \sigma_0^2 I_e^{-1} . \quad (4)$$

Owing to the manner in which surface brightness is defined (Appendix A), c_1 is a constant. It is now easy to verify that if $M/L \propto L^{0.2}$ and c_2 is also constant for all galaxies, we directly obtain the equation of the fundamental plane. This was first pointed out by Faber et al. (1987). However, this is only one possibility. The fundamental plane equation could also be derived by assuming M/L to be constant, combined with a systematic variation of c_2 relative to the fundamental variables. This variation is explored for King models in Appendix A.

To make the analysis in this paper as transparent as possible, it is highly desirable to choose a well-suited orthogonal coordinate system in the 3-space of the observable parameters $\log \sigma_0^2$, $\log r_e$, and $\log I_e$. The following coordinate system turns out to be both physically meaningful (see below) and easy to remember:

$$\kappa_1 \equiv (\log \sigma_0^2 + \log r_e)/\sqrt{2} , \quad (5)$$

$$\kappa_2 \equiv (\log \sigma_0^2 + 2 \log I_e - \log r_e)/\sqrt{6} , \quad (6)$$

$$\kappa_3 \equiv (\log \sigma_0^2 - \log I_e - \log r_e)/\sqrt{3} . \quad (7)$$

Specifically, $\kappa_1 \propto \log (M/c_2)$, $\kappa_2 \propto \log (c_1/c_2)\ (M/L) I_e^3$ and $\kappa_3 \propto \log (c_1/c_2)\ (M/L)$. In words, κ_1 is proportional to the logarithm of the mass, κ_3 is proportional to the logarithm of M/L, and κ_2 is proportional to the logarithm of $(M/L) I_e^3$. All three parameters are defined within the luminous parts of the galaxies.

The κ coordinate system was obtained by a simple *orthogonal coordinate transformation* (i.e., a rotation), applied to the observed parameters. Anything other than a pure rotation might introduce spurious correlations between the new axes and would also destroy the advantage of working with parameters that are quasi-normalized. The particular choice of orthogonal coordinate transformation was dictated by our primary desire that the first parameter be a simple measure of galaxy size: $\kappa_1 \propto \log M$. We then wanted κ_3 to combine with κ_1 to show the fundamental plane edge-on. This forces κ_3 to be some combination of $\log M$ and $\log (M/L)$, as $M/L \propto L^{1/5} \propto M^{1/6}$ is the defining equation of the plane. Since $\log M$ had already been used, $\kappa_3 \propto \log M/L$ was the most logical remaining choice. The direction of κ_2 was then fixed by the need to be orthogonal to both κ_1 and κ_3. The variance in κ_1 and κ_2 is ≈ 0.4, similar to that for the observable parameters $\log \sigma^2$, $\log r_e$, and $\log I_e$. In contrast, κ_3 has a much smaller variance (see Fig. 1), owing to the fact that the dependence of M/L on M is so weak ($M/L \propto M^{1/6}$) and that the scatter in M/L at a given M is rather small.

In this new coordinate system, the κ_1/κ_2 projection is close to being a face-on view of the fundamental plane, while the κ_1/κ_3 projection gives an edge-on view of the plane. The third projection κ_2/κ_3 adds little additional information and is not employed here. The κ_1/κ_2 projection would view the fundamental plane exactly face-on if $r_e \propto \sigma_0^2 I_e^{-1}$. The fact that the κ_1/κ_2 plane is slightly inclined to the fundamental plane has no significant consequences for our analysis. Obviously we could have used a coordinate transformation which would have given us a direct face-on view of the fundamental plane, but at the cost of physically obscure coordinate axes. The κ-coordinate system is the best system produced by orthogonal transformation from the original variables, in which all coordinates are physically meaningful *and* in which the fundamental plane is projected exactly edge-on using one pair of coordinates.

Figure 1 shows the distribution of the "normal" Virgo and Coma ellipticals in projection onto κ_1/κ_2 (fundamental plane face-on) and onto κ_1/κ_3 (fundamental plane edge-on). (Note that Coma galaxies do not have v/σ_0 estimates and, hence, are

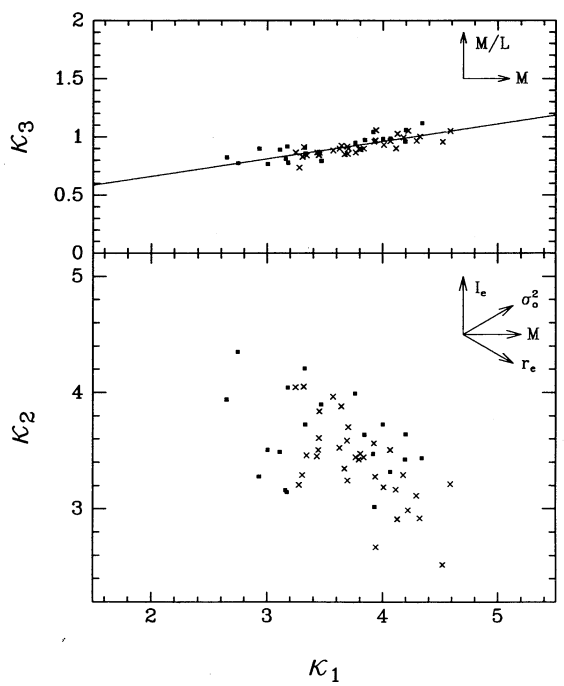

FIG. 1.—The distribution of elliptical galaxies in the Virgo Cluster and the Coma Cluster in the 3-space of the basic global parameters: central velocity dispersion (σ_o^2), surface brightness [$\log I_e = -0.4(SB_e - 27)$], and effective radius r_e. The coordinate system (κ_1, κ_2, κ_3) has been chosen to emphasize the fundamental plane while retaining physically meaningful variables: $\kappa_1 \propto \log M$, $\kappa_2 \propto \log (M/L) I_e^3$ and $\kappa_3 \propto \log M/L$. (*a*) *Upper panel:* the edge-on view of the plane occupied by Virgo (*closed boxes*) and Coma (*crosses*) ellipticals. The fundamental plane defined by the Virgo galaxies ($\kappa_3 = 0.15\ \kappa_1 + 0.36$) is shown by the straight line. (*b*) *Lower panel:* nearly face-on view of the plane.

not specifically analyzed further in this paper.) For both clusters the photometric and kinematic data were taken from Faber et al. (1989), and their distances were derived consistently with the prescription given in § 2; i.e., group redshifts were corrected to the centroid of the Local Group (redshifts of 1035 km s^{-1} for Virgo and 6900 km s^{-1} for Coma). Distances were then calculated arbitrarily using $H_0 = 50$ km s^{-1} Mpc^{-1}. From Figure 1 it is evident that the physical properties of Coma ellipticals, as are Virgo ellipticals, are well constrained to a plane. The slight systematic offset between the planes defined by these two clusters is entirely due to the conservative approach we have adopted for this paper, in which we have purposefully neglected all possible peculiar motions (including the well-known motion of the Local Group relative to the Virgo cluster). The fundamental plane defined by the Virgo galaxies (eq. [1]) is drawn in the upper panel of Figure 1, and has the form $\kappa_3 = 0.15\kappa_1 + 0.36$ (or, since $\kappa_1 \propto \log M$ and $\kappa_3 \propto \log M/L$, $M/L \propto M^{0.15} \propto L^{0.2}$; again, this interpretation is strictly valid only if the structure constant c_2 does not vary with M).

Cluster galaxies are used for Figure 1 because they are well observed and are all at the same distance. There is other evidence that cluster ellipticals are generally quite homogeneous in their physical properties (Sandage & Visvanathan 1978; Dressler et al. 1987), *with the possible exception of the Perseus Cluster* (see also Lucey et al. 1991). Field galaxies may not show such small scatter, owing both to distance errors and to the possibility that they are less homogenous than cluster galaxies.

3.2. *Parametrizing Physical Processes*

The present structure of galaxies must be due to some combination of initial conditions and the actions of physical processes that have occurred since the beginning of galaxy formation. The major physical processes we can readily identify are: energy dissipation in the baryonic component, merging/accretion, supernova-driven mass loss, stripping of outer parts due to tidal forces, and stripping of gas due to ram pressure. Here we derive how these processes affect the location of the luminous parts of galaxies in κ-space:

1. *Energy dissipation.*—Energy dissipation in the baryonic component is clearly one of the most important processes that determine the structure of present-day galaxies, as the baryonic density of protogalaxies was most likely much lower at the turn-around time than it is today (e.g., White & Rees 1978; Faber 1982; Blumenthal et al. 1984). Energy dissipation presumably continues to play an important role in the formation of ellipticals through ongoing gaseous merging (e.g., Kormendy 1990; see below). Luminous ellipticals are baryon-dominated (Faber et al. 1987), and energy dissipation conserves both baryonic mass and M/L. As viewed in κ-space, these changes correspond to $\kappa_1 =$ constant, $\delta\kappa_2 = \sqrt{3/2}\,\delta \log I_e$ and $\kappa_3 =$ constant. That is, energy dissipation moves galaxies within the fundamental plane and parallel to the κ_2 axis.

2. *Merging.*—Merging between galaxies or among their progenitors most likely occurs over a large redshift interval (but primarily at redshifts greater than 1) and in a hierarchical manner. For this paper we assume a cold dark matter (CDM) density fluctuation spectrum with $h = 0.5$, $\Omega = 1$ (Blumenthal et al. 1984). A merging hierarchy can then be parametrized in terms of the *total* mass of the final galaxy (M) and the mass density fluctuation $\delta\rho/\rho$ out of which the galaxy formed (e.g., Gott & Rees 1975; White & Rees 1978). These authors (cf. also Faber 1984) find the following relationships linking the final structural parameters of a collapsed, *dissipationless* galaxy of given M and $\delta\rho/\rho$: $r \propto \delta^{-1} M^{1/3}$, $\sigma \propto \delta^{1/2} M^{1/3}$, $\rho \propto \delta^3$, and $I \propto \delta^2 M^{1/3}(M/L)^{-1} \propto \delta^2 M/L^{1/6}$. The parameters r, σ, ρ, and I are, respectively, the characteristic radius, velocity dispersion, mass density, and surface brightness of the galaxy in the absence of dissipation.

To proceed further, we assume that M may be replaced by $M_{\rm Bary}$, the baryonic mass, in some fixed ratio, e.g., $M = 10M_{\rm Bary}$, and that dissipation shrinks the observed *baryonic* radii relative to the radii without dissipation also by a fixed amount. The above relations then still hold, but the parameters now refer to the visible baryonic matter rather than the (presumed dark) dissipationless matter. The substitution $M/L \propto L^{1/5} \propto M^{1/6}$ accounts for final step in the last relation above. Furthermore, we assume that L refers to a relatively old stellar population, to be consistent with the absence of obvious star formation in most present-day ellipticals.

The simple CDM merging hierarchy thus predicts that collapsed, dissipated galaxies obeying the above assumptions should follow these scaling laws. Since $M/L \propto L^{1/5}$ *is* the equation of the fundamental plane, setting $L^{1/5} \propto M^{1/6}$ above ensures that the merging hierarchy will lie within the fundamental plane. We note that physics can provide the justification of the relations linking r, σ, and ρ to M. In contrast, the linkage of I with M is only empirical, as the absence of a rigorous theory of star formation precludes a physical justification for this relation.

In terms of the parameters κ_1 and κ_2, we find from their definitions that $\kappa_1 = 1/\sqrt{2} \log M_{\rm Bary} + K_1$ and $\kappa_2 = 1/\sqrt{6} \log [(M/L)I_e^3] + K_2 = 2.45 \log (\delta\rho/\rho) + 0.27 \log M_{\rm Bary} + K_2$. The horizontal normalization constant K_1 has been determined assuming that the galaxies have $r^{1/4}$ luminosity distributions and isotropic velocity dispersions, such that $\kappa_1 = 3.5$ corresponds to $M_{\rm Bary} \approx 10^{11}\,M_\odot$, or $M_{\rm dark} \approx 10^{12}\,M_\odot$. The vertical normalization K_2 is chosen arbitrarily to make the 2.5 σ locus for $\delta\rho/\rho$ pass close to the center of the distribution for giant ellipticals in the plane. Values of $\delta\rho/\rho$ versus M have been read from the $\Omega = 1$, $h = 0.5$ model from Figure 1 of Blumenthal et al. (1984). The final equations for the CDM merging hierarchy are then $\kappa_1 = 1/\sqrt{2} \log M_{\rm Bary} + 2.79$ and $\kappa_2 = 2.45 \log (\delta\rho/\rho) + 0.27 \log M_{\rm Bary} + 0.51$, with $M_{\rm Bary}$ in units of $10^{10}\,M_\odot$.

A rough vector direction is sketched in Figure 2*b*, and theoretical trajectories for 2.5 σ and 1.0 σ fluctuations are drawn in Figure 4. Since $\delta\rho/\rho$ is itself a declining function of $M_{\rm Bary}$, κ_2 changes little with κ_1, and the trajectory is nearly horizontal in these figures.

3. *Galactic winds.* Galactic winds become increasingly important at lower galactic masses (e.g., Larson 1974). Winds may be important for understanding the diffuse nature of dwarf galaxies as well as the overall trend between metallicity and mass of hot stellar systems (Larson 1974; Brocato et al. 1990; Yoshii & Arimoto 1987). As long as the galaxy is baryon-dominated and mass loss is not severe, it is reasonable to expect that mass loss reduces M but probably conserves M/L. Adiabatic mass loss also conserves the product $r_e\sigma_0$ (Hills 1980; Vader 1986). Therefore, a baryon-dominated galaxy experiencing wind-driven mass loss will move according to $\delta\kappa_1 = 1/\sqrt{2}\,\delta \log M$, $\delta\kappa_2 = 9/\sqrt{6}\,\delta \log M$, and $\kappa_3 =$ constant. This is a very steep, downward vector as projected onto the fundamental plane (see Fig. 2*b*). In the edge-on view

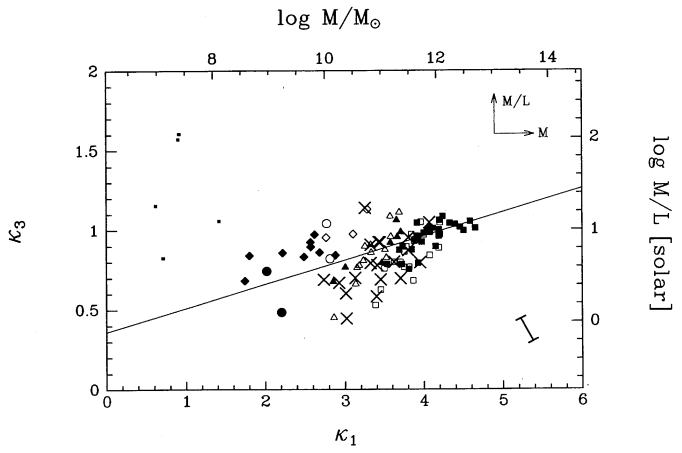

FIG. 2a

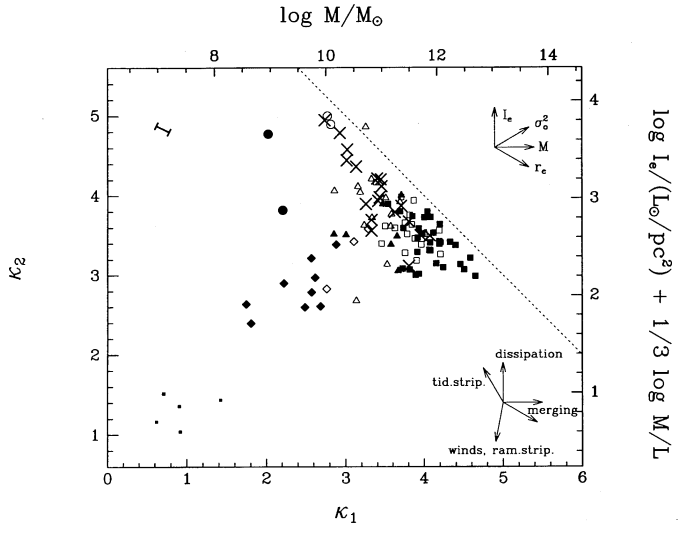

FIG. 2b

FIG. 2.—Distribution of all types of hot stellar systems in κ-space as defined in Fig. 1 and in the text. The values of the corresponding physical parameters are given on the opposite sides of the figures [masses M were determined from $M = 5G^{-1}\sigma_o^2 r_e$ and are given in solar units; mean effective surface brightnesses $\langle I\rangle_e$ were derived from $\log\langle I\rangle_e = -0.4(SB_e - 27)$ and refer to units of $L_\odot/\mathrm{pc}^2$; luminosities L are given by $L = 2\pi\langle I\rangle_e r_e^2$ in solar units; for further details, see Appendix 1]. The plane occupied by hot stellar systems is again shown in (*a*) edge-on and (*b*) face-on view. Squares denote giant ellipticals ($M_T < -20.5$ mag), triangles denote ellipticals of intermediate luminosity (-20.5 mag $< M_T < -18.5$ mag), circles denote compact galaxies and diamonds denote bright dwarf galaxies ($M_T > -18.5$) with known kinematics. Open symbols are galaxies that are rotationally flattened; filled symbols are galaxies that have anisotropic kinematics. Bulges are represented by only one symbol (*crosses*), as all those for which internal kinematics has been obtained appear to be rotationally flattened (see Table 1). The five small filled squares refer to Fornax (which is anisotropic) and four other dwarf spheroidal companions of the Galaxy for which no spatially resolved kinematics are available. The arrows in the upper right of the lower panel indicate the directions in which the basic global parameters of hot stellar systems increase. The arrows in the lower right of the lower panel sketch how the major processes move objects in the plane (tid. strip = tidal stripping, ram. strip = ram pressure stripping). The range of directions for merging is approximate; a more detailed treatment of CDM mergers is given in Fig. 4. An error bar corresponding to a distance uncertainty of $\pm 30\%$ is given in the lower right corner of (*a*) and the upper left corner of (*b*). The diagonal dashed line highlights the area in this plane not occupied by hot stellar systems.

(Fig. 2*a*), the galaxy moves horizontally to the left, such that galaxies that were once in the plane will move slightly above it.

As the potential of a galaxy gradually becomes dominated by dark matter, M = constant, M/L and κ_3 both increase, and further wind-driven expansion in r_e is suppressed (Dekel & Silk 1986). Such may be the case for the most diffuse dwarf spheroidal galaxies if these are dark-matter dominated (Faber & Lin 1983; Aaronson 1983). In the face-on view, the mass-loss vector becomes even steeper, and, in the edge-on view, such mass loss carries galaxies vertically upward and away from the fundamental plane.

4. *Tidal stripping.*—To a first approximation, stripping of stars from the outer parts of a galaxy will leave σ_0 approximately constant (σ_0 will decline slightly as the galaxy expands), reduce r_e, and make I_e brighter (Faber 1973; Nieto & Prugniel 1987). Schematically, $\sigma_0 \approx$ const., $I_e \propto r_e^{-1}$, $\delta\kappa_1 = 1/\sqrt{2}\,\delta \log M$, $\delta\kappa_2 = -\sqrt{3/2}\,\delta \log M$, and κ_3 = constant. As with galactic winds, there is a slight motion out of the fundamental plane since M/L is conserved.

5. *Ram pressure stripping.*—This process has been proposed by Faber & Lin (1983) as a means to transform irregular galaxies into dwarf ellipticals by removing the gaseous component. If the gas removal happens slowly compared to the dynamical time scale, the baryonic part of the object adiabatically inflates as in case of wind-driven mass loss (see number 3 above).

To summarize, within the κ_1/κ_3 plane, merging tends to move galaxies in a direction nearly perpendicular to dissipation and winds, which themselves operate in opposite directions. Tidal stripping moves galaxies at an angle to all of the above effects, but closest to the direction of dissipation. Within the κ_1/κ_3 plane, the fundamental plane is canted at a slight angle, reflecting the apparent overall change in M/L with M. The fact that three of the physical processes do not change M/L while the other two change it only under extreme circumstances means that most processes tend to broaden the plane only slightly, rather than thicken it markedly.

Two additional effects also affect the distribution of galaxies in κ-space: distance errors and changes in the c_2 structure parameter. It D is distance, then $\delta\kappa_1 = 0.707\delta \log D$, $\delta\kappa_2 = -0.408\delta \log D$ and $\delta\kappa_3 = -0.577\delta \log D$. Thus distance errors move galaxies along lines of fairly steep negative slope in both the κ_1/κ_2 and κ_1/κ_3 projections.

The structure parameter c_2 is assumed to be independent of galaxy type in deriving the κ-dependencies above. However, systematic variation in galaxy luminosity profiles are observed as a function of position in κ-space. To gain some insight into the importance of this effect, we compute variations in c_2 using a series of King models (Appendix A). The only κ parameter notably impacted is κ_3 (M/L), and the consequences are discussed below where needed.

4. THE DISTRIBUTION OF HOT STELLAR SYSTEMS WITH RESPECT TO THE FUNDAMENTAL PLANE OF ELLIPTICAL GALAXIES

4.1. *Galaxy Types in the Edge-on Projection*

Figures 2*a* and 2*b* show the distributions in κ-space of the six kinds of hot galaxies defined in § 2—giant ellipticals, intermediate ellipticals, compact ellipticals, bulges of disk galaxies, bright dwarf ellipticals, and faint dwarf spheroidals—plotted in the κ coordinate system. Each galaxy type is plotted with a

TABLE 2

κ PARAMETERS FOR HOT STELLAR SYSTEMS

Galaxy (1)	κ_1 (2)	κ_2 (3)	κ_3 (4)	$\delta\kappa_3$ (5)
Giant Ellipticals				
NGC 315	4.652	2.988	1.010	−0.047
NGC 584	3.818	3.756	0.766	−0.167
NGC 636	3.501	3.617	0.756	−0.129
NGC 720	3.977	3.525	0.924	−0.033
NGC 777	4.397	3.377	1.033	0.014
NGC 821	3.902	3.183	0.932	−0.013
NGC 1052	3.783	3.518	0.893	−0.034
NGC 1395	4.003	3.517	0.968	0.007
NGC 1399	4.045	3.798	0.991	0.025
NGC 1404	3.708	3.982	0.795	−0.121
NGC 1407	4.209	3.262	1.044	0.053
NGC 1549	3.736	3.592	0.895	−0.025
NGC 1600	4.506	3.069	0.993	−0.043
NGC 1700	3.869	3.940	0.680	−0.261
NGC 2300	4.077	3.408	1.016	0.014
NGC 2974	3.880	3.460	0.929	−0.013
NGC 3091	4.193	3.392	0.999	0.010
NGC 3557	4.194	3.561	0.885	−0.104
NGC 3607	3.963	3.383	1.048	0.064
NGC 3610	3.388	4.171	0.528	−0.340
NGC 3613	3.757	3.657	0.861	−0.063
NGC 3640	3.629	3.592	0.797	−0.107
NGC 3904	3.692	3.802	0.872	−0.041
NGC 4125	4.079	3.308	0.839	−0.133
NGC 4168	3.893	3.000	0.937	−0.007
NGC 4261	4.120	3.531	1.009	0.031
NGC 4365	3.918	3.471	1.042	0.094
NGC 4374	4.002	3.726	0.980	0.019
NGC 4406	4.066	3.316	0.983	0.013
NGC 4472	4.194	3.423	0.960	−0.029
NGC 4494	3.456	3.396	0.624	−0.254
NGC 4589	3.914	3.290	0.960	0.013
NGC 4621	3.844	3.636	0.971	0.034
NGC 4636	3.931	3.014	0.957	0.008
NGC 4649	4.200	3.639	1.058	0.038
NGC 4697	3.757	3.280	0.764	−0.159
NGC 4889	4.588	3.213	1.051	0.003
NGC 5322	3.933	3.586	0.789	−0.161
NGC 5576	3.537	3.896	0.784	−0.107
NGC 5846	4.242	3.094	1.084	0.058
NGC 6411	3.815	3.070	0.752	−0.180
NGC 6909	3.726	3.082	0.783	−0.136
NGC 7507	3.851	3.739	0.874	−0.064
NGC 7619	4.330	3.416	1.040	0.030
NGC 7626	4.155	3.146	0.894	−0.089
NGC 7785	4.209	3.411	0.971	−0.021
IC 1459	4.082	3.729	0.984	0.012
IC 4296	4.458	3.134	1.016	−0.013
Intermediate Ellipticals				
NGC 1379	3.528	3.136	0.824	−0.065
NGC 1439	3.666	3.051	0.954	0.044
NGC 2694	3.156	4.117	0.763	−0.070
NGC 3156	3.136	2.676	0.659	−0.171
NGC 3193	3.583	3.767	0.955	0.058
NGC 3377	3.234	3.627	0.805	−0.040
NGC 3379	3.509	3.970	0.874	−0.012
NGC 3608	3.654	3.489	1.061	0.152
NGC 3818	3.575	3.613	1.084	0.187
NGC 4278	3.691	3.920	1.109	0.195
Intermediate Ellipticals				
NGC 4291	3.710	4.004	0.985	0.068
NGC 4387	2.855	3.516	0.676	−0.112
NGC 4473	3.469	3.897	0.792	−0.089
NGC 4478	3.182	4.042	0.776	−0.061
NGC 4551	3.006	3.506	0.765	−0.046
NGC 4564	3.332	3.722	0.857	−0.003
NGC 4660	3.327	4.207	0.905	0.046
NGC 4742	2.860	4.062	0.450	−0.339
NGC 5831	3.578	3.383	0.917	0.021
NGC 5845	3.253	4.857	0.896	0.048
Bright Dwarf Ellipticals				
NGC 147	1.804	2.396	0.839	0.208
NGC 185	1.745	2.638	0.682	0.060
NGC 205	2.219	2.898	0.856	0.163
NGC 3605	3.106	3.423	0.975	0.149
NGC 3641	3.284	3.581	1.128	0.275
NGC 4431	2.765	2.830	0.953	0.178
NGC 4467	2.571	3.216	0.903	0.157
NGC 4515	2.884	3.388	0.842	0.049
IC 794	2.687	2.607	0.859	0.096
IC 3393	2.574	2.786	0.905	0.159
UGC 7436	2.489	2.597	0.831	0.098
V 351	2.621	2.970	0.971	0.218
Compact Ellipticals				
NGC 221	2.022	4.773	0.742	0.079
NGC 4486B	2.774	4.999	1.040	0.264
NGC 5846A	2.815	4.892	0.820	0.038
IC 767	2.207	3.822	0.485	−0.206
Dwarf Spheroidals				
For	1.421	1.433	1.057	0.483
Scl	0.714	1.515	0.826	0.358
Car	0.622	1.160	1.155	0.701
Dra	0.905	1.356	1.570	1.075
UMi	0.919	1.037	1.605	1.107
Bulges				
NGC 16	3.455	4.117	0.687	−0.191
NGC 474	3.410	3.935	0.777	−0.094
NGC 936	3.626	3.793	0.797	−0.106
NGC 1175	3.707	3.872	0.694	−0.222
NGC 1553	3.400	4.214	0.582	−0.288
NGC 2549	3.014	4.443	0.602	−0.211
NGC 2639	3.806	3.112	0.950	0.019
NGC 2778	3.255	3.896	1.137	0.289
NGC 2880	3.326	3.695	0.790	−0.068
NGC 3300	3.327	3.560	0.905	0.046
NGC 3115	3.446	4.204	0.921	0.044
NGC 4026	2.926	4.785	0.669	−0.130
NGC 4036	3.428	3.979	0.922	0.048
NGC 4111	2.738	4.946	0.688	−0.083
NGC 4169	3.804	3.674	0.871	−0.059
NGC 4281	4.074	3.497	1.044	0.073
NGC 4594	3.956	3.501	0.793	−0.160
NGC 5380	3.132	4.364	0.698	−0.132
NGC 7332	3.020	4.577	0.445	−0.368

NOTES.—Col. (1).—Galaxy name, as in Table 1.
Col. (2).—$\kappa_1 \equiv (\log \sigma_0^2 + \log r_e)/(2)^{1/2}$.
Col. (3).—$\kappa_2 \equiv (\log \sigma_0^2 + 2 \log I_e - \log r_e)/(6)^{1/2}$.
Col. (4).—$\kappa_3 \equiv (\log \sigma_0^2 - \log I_e - \log r_e)/(3)^{1/2}$.
Col. (5).—$\delta\kappa_3 \equiv \kappa_3 - 0.36 - 0.15\kappa_1$.

separate symbol, as defined below. In addition, galaxies that are anisotropic are plotted with closed symbols, while isotropic, rotationally flattened galaxies (except bulges) are plotted with open symbols. (All bulges considered here are rotationally flattened and are plotted with crosses.)

The edge-on view of the fundamental plane is shown in Figure 2*a*. It is striking that hot galaxies with anisotropic velocity distributions (*closed symbols*) tend to be found at *both* high and low values of κ_1 (mass). This duality was first noted by BN90. Hot stellar systems that are rotationally flattened (*open symbols and crosses*) tend to be found in between these two extremes and have more scatter around the fundamental plane. In the parameter range $2.5 < \kappa_1 < 4.5$, where Virgo ellipticals show little scatter, all the objects of our sample have considerably more scatter relative to the fundamental plane.

To aid in interpreting this scatter, we plot the residuals, $\delta\kappa_3$, relative to the fundamental plane against degree of anisotropy $(v/\sigma_0)^*$ in Figure 3 (values of $\delta\kappa_3$ are given in Table 2). There are hints that the residuals are not completely random. Bulges tend to lie systematically below the fundamental plane, while dwarf galaxies tend to lie above it. These points will be discussed further below.

At least part of the scatter in Figure 2*b* is probably due to distance errors. Typical errors are in the range 15%–30% (0.06–0.12 dex) for distances based on redshift only, owing to peculiar motions (Burstein 1990). These will translate into errors in the κ parameters as 0.04–0.08, 0.02–0.04, and 0.03–0.07, respectively.

In terms of specific kinds of galaxies:

1. Bright dwarf ellipticals (*diamonds*) seem to follow their own relationship parallel to the fundamental plane but offset from it by $\sim +0.15$ in κ_3. Examination of Table 1 shows that seven of the 12 bright dwarf galaxies are in Virgo, so distance errors can be ruled out. Similarly, very large errors of 35% in σ_0 (measured too high) or 0.65 mag in M_T (measured too low) would be required to produce the effect and would have to exist uniformly for all dwarfs. This is also unlikely. On the one hand, this offset could reflect a genuinely higher M/L for bright dwarfs. Alternately, c_2 may be different. However, analysis of King galaxy models (Appendix A) indicates that, by ignoring differences in c_2, we have, if anything, *under* estimated M/L, not the reverse. Hence, it is probable that the apparent offset of the dwarf galaxies from the fundamental plane is real. This offset is an unexpected new discovery that may hold an important clue to the dynamical structure and/or stellar populations of bright dwarfs.

2. The five low-luminosity dwarf spheroidals (*small squares*), including Fornax, stand off the plane strongly owing to higher M/L. The natural decline in M/L with lower luminosity appears to be reversed at $M_T \approx -15$ mag, which evidently marks the onset of extreme depletion of baryonic matter relative to dark matter.

3. The four compact ellipticals (*circles*) scatter widely but in the mean follow the plane. The reason for this extra scatter is not known.

4. Bulges (*crosses*) follow the fundamental plane but lie systematically ~ 0.1 in κ_3 below it. This may reflect a number of possible systematic differences between bulges and ellipticals, including: (i) a genuinely lower M/L due to more recent star formation; (ii) higher values of c_2; (iii) larger than average measurement errors owing to disk contamination; (iv) perturbation of the gravity field by the disk mass; and (v) extra support from rotation not included in the mass estimate. This last effect is estimated using the tensor virial theorem (Appendix B) and appears to be able to account for about one-half of the observed offset.

5. Isotropic luminous ellipticals (*open squares and triangles*) tend to scatter around the fundamental plane somewhat more than do their anisotropic counterparts, with a hint of skewing towards lower M/L. Two of the galaxies with lowest M/L are NGC 3156 and NGC 4742, both of which are known to have recent or ongoing star formation (Burstein et al. 1988a; Gregg 1989). One other galaxy with low M/L, NGC 4494, is known to have peculiar core kinematics (Bender 1988b).

These three galaxies may simply be the most extreme examples of more widespread phenomena present at lower amplitude in the remaining objects, although not all galaxies may exhibit ongoing star formation (Bertola et al. 1993a,b). Moreover, rotation contributes support in some of these galaxies which could produce a net offset of a few hundreths in $\delta\kappa_3$ for the group (Appendix B). These effects together seem able to account for the distribution of isotropic rotators about the plane.

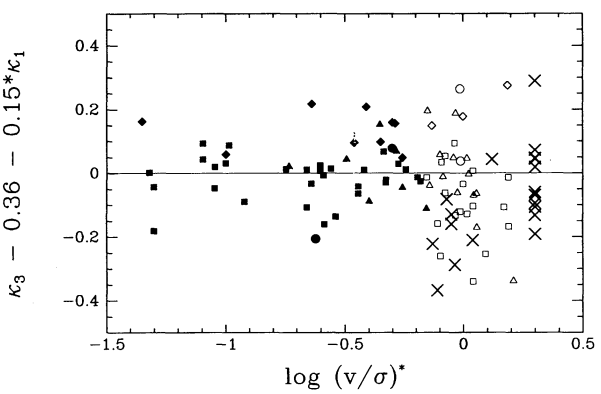

FIG. 3.—The residual of a galaxy relative to the fundamental plane as projected along the κ_3 axis, defined as $\kappa_3 - 0.36 - 0.15\kappa_1$, plotted vs. the degree of anisotropy of the system, defined as $(v/\sigma_o)^*$. Symbols are the same as in Fig. 2. On the vertical scale a change by 1 unit corresponds to a change in log M/L of 2.12 if L is held constant, or alternately a change of 1.73 if M is held constant. Four dwarf spheroidal galaxies are missing from this diagram because they lack measured values of $(v/\sigma_o)^*$. Bulges (*crosses*) tend to lie below the fundamental plane while bright dwarf ellipticals (*diamonds*) tend to lie above it. Bulges, for which no measure of anisotropy was available are plotted at log $(v/\sigma)^* = 0.3$.

4.2. *The Distribution of Luminous Ellipticals within the Fundamental Plane*

The face-on view of the fundamental plane (Fig. 2*b*) offers complementary information to that provided by the edge-on view. As discussed in § 3, most of the physical processes expected to be important for hot stellar systems move galaxies *within* this plane far more than they move them *out* of it. As such, it is not surprising that galaxies distribute themselves more widely within the plane than perpendicular to it.

Figure 4 replots Figure 2*b* but this time including 292 ellipticals not already used in this paper from the seven Samurai survey of Faber et al. (1989). The addition of these other galaxies strengthens a conclusion, hinted at in Figure 2*b*, that the general region occupied by luminous ellipticals (*squares and triangles*) is delimited by the line $\kappa_1 + \kappa_2 \leq 7.8$. In terms of the structural properties, this implies $r_e \sigma_0^{7.46} I_e^{-2.72} \leq$ constant. The fact that this constraint involves all three physical properties of hot stellar systems means that both the density and the

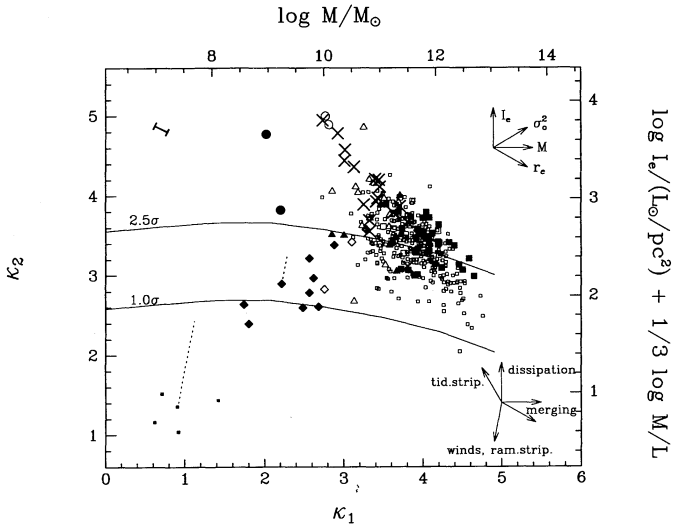

FIG. 4.—The κ_1/κ_2 plane for hot stellar systems. Galaxies are repeated from Fig. 2 using the same symbols. Parameters for an additional 292 elliptical galaxies from Faber et al. (1989) are plotted as small open squares, for which no degree of anisotropy is implied. Lines represent $\kappa_1 - \kappa_2$ loci for galaxies of different mass arising from a CDM density fluctuation spectrum with different degrees of overdensity, $n\sigma$. Two values of $n\sigma$ are shown: 1.00 σ and 2.5 σ. CDM loci have been normalized horizontally and vertically as described in the text. An error bar corresponding to a distance uncertainty of $\pm 30\%$ is given in the upper left corner.

total mass of the progenitors of luminous ellipticals are mutually constrained; in effect, there is an upper limit to the amount of dissipation for a given mass. The reason(s) for this are unknown, but the existence of this limit must be satisfied by any successful model of elliptical galaxy formation.

As noted, intermediate ellipticals (*triangles*), like bulges, are predominantly rotationally flattened (cf. DEFIS; BN90). Recent detailed photometry has shown that many intermediate luminosity ellipticals harbor weak stellar disks and have radio properties similar to those of S0 galaxies (Bender et al. 1989). Ellipticals of intermediate luminosity share enough common properties with bulges that the distinction between these two kinds of hot stellar systems is likely to be an artifact of morphological classification: Intermediate "ellipticals" simply have systematically lower disk-to-bulge ratios than galaxies classified as S0's (Burstein 1978; Bender et al. 1989; Rix & White 1990).

Giant ellipticals (*squares*), in contrast, show a large range in velocity dispersion anisotropy and specific angular momentum (DEFIS; BN90), indicating that these galaxies do not form a uniform group. Some of these contain faint stellar disks, are rotationally flattened, and are radio quiet, similar to S0 galaxies and intermediate ellipticals. It is plausible that these are just the brighter end of elliptical galaxies with significant disks (Bender 1990). On the other hand, many giant ellipticals, especially "boxy" ellipticals, show not only anisotropic velocity dispersions but also various evidence for peculiar dynamics (Franx & Illingworth 1988; Jedrzejewski & Schechter 1988; Bender 1988b, 1990). As discussed in the above papers, stellar-dominated mergers are the most likely source of these phenomena. Moreover, Bender (1991) has pointed out that boxy ellipticals are on average more luminous than disky ellipticals which, combined with the above discussion, also implies that peculiar dynamics and luminosity are correlated for ellipticals. This suggests that the luminous ellipticals as a group constitute a *merging continuum*, as explained in more detail below.

The key concept behind such a continuum is the idea that the importance of gas during the merger process declines with galaxy mass, while the importance of stars increases; i.e., a progression from largely gaseous, dissipational mergers to largely stellar, dissipationless mergers (cf. Kormendy 1989, 1990). This decline in gas might occur because of gradual transformation of gas to stars as galaxies are assembled, although this is not strictly required (see below). The process *cannot* be purely a function of mass, however, as we find both anisotropic *and* rotationally flattened galaxies at similar mass. Rather, the relation to mass must be only statistical and is influenced by the specific details of the galaxy formation process in each individual galaxy.

CDM theory may provide some indirect support for such a continuum. The CDM merging trajectory within the fundamental plane is drawn in more detail in Figure 4. CDM has been compared to ellipticals before, but this comparison is new because it looks at the merging trajectory within the full three-dimensional κ-space itself, rather than in a skewed projection. Earlier comparisons (e.g., Faber 1982; Silk 1983; Blumenthal et al. 1984) have shown fair agreement with CDM but have used submaximal projections, which can falsely improve the agreement between theory and data.

In the present more stringent test, CDM does not at first sight appear to match the distribution of luminous ellipticals galaxies very well. The CDM trajectory (at constant value of overdensity $n\sigma$) is nearly horizontal, the observed galaxy distribution (*squares and triangles*) is tilted noticeably downward and to the right, bounded as described above. The galaxy locus is broad, but this can plausibly be explained by invoking variable amounts of dissipation in different galaxies. The important issue is the overall difference in slope.

This discrepancy could be solved by dismissing CDM altogether in favor of some other theory. Or, more luminous ellipticals may come from lower σ perturbations than smaller ellipticals. However, there is a third possibility of interest here, namely, the idea that the degree of dissipation does not remain constant versus galaxy mass. The sense is such that the amount of dissipation would have to decrease at higher masses. This is interesting because it is at least qualitatively consistent with a declining role for gas in more luminous ellipticals. With less gas and more stars, radiative loss of energy would decline.

We are aware that this question is complicated, as dissipation (i.e., entropy increase) can occur even without radiative losses. Stars can exchange energy and angular momentum with each other and with the dark matter (e.g., by dynamical friction of dense cores against halos; Barnes 1988). Such processes could alter the degree of concentration and the shape of the luminosity profile. The systematic difference between the core profile shape of small versus large ellipticals (Lauer 1985; Kormendy 1985, 1987) may actually testify to such a process. N-body models, both dissipationless *and* with dissipation, will be needed to futher investigate these possibilities. We merely note here that the obvious discrepancy with CDM might be resolved if gas indeed plays a smaller role in more massive mergers.

These considerations lead us to speculate that *the anisotropy parameter* $(v/\sigma_0)^*$ *is a crude measure of the ratio of baryonic mass in* (*cold*) *gas to mass in stars at the time when the last major merger occurred.* This might be termed a *gas/stellar* (*GS*) *continuum.* As stars, rather than the dissipational gas, dominate the

baryonic mass, the more the final stellar system appears to retain a memory of the dynamics of its original precursor galaxies, plus the geometries of the orbital encounters. These now persist together in the form of particular anisotropies and/or peculiar core kinematics which can last a long time since the last encounter (otherwise the high fraction of luminous ellipticals exhibiting peculiar core kinematics cannot be accounted for, Bender 1990). N-body simulations could be valuable in determining quantitatively how quickly this earlier memory is erased as a function of gas fraction and star formation efficiency.

It might be objected that largely stellar mergers would erase the correlation between mass and mean metallicity that extends to even the most massive ellipticals (Burstein et al. 1988b). However, measures of metallicity (i.e., the Mg_2 index) actually correlate more closely with central velocity dispersion than they do with total mass (Dressler et al. 1987; Bender 1992). The behavior of central velocity dispersion is quite uncertain in mergers, owing to the current lack of knowledge of the effectiveness of dissipation in the merger process. It is conceivable that σ_0 may remain quite constant within a given galaxy, which would remove all contradiction. We explore the relationship of the stellar populations of hot stellar systems to their physical properties in future papers of this series.

We note that the idea of a GS continuum among ellipticals also fits naturally with the concept of a *merging hierarchy*, in which larger galaxies along the elliptical sequence are built up out of smaller ones, and gas is converted to stars along the way. In this view, small ellipticals (plus a few spirals) are the direct progenitors of giant ellipticals, and the small ellipticals left today are simply those that managed to escape further merging. The elliptical sequence would thus be a temporal sequence as well as a gas-to-stars sequence, with the giants forming after (and partially out of) the smaller ones.

While this is certainly a consistent and attractive picture (we mention it as one possibility above), it is not, strictly speaking, a necessary one. Instead, large and small ellipticals may have been built up separately on parallel tracks, from similar processes perhaps, but at different rates and different times, and with different final gas/star ratios. The idea of a GS continuum as we envision it does not strictly require the temporal evolution of small ellipticals to large ones.

4.3. *The Distribution of Bulges within the Fundamental Plane*

In the face-on view of the plane, bulges (*crosses*) overlap the distribution of intermediate ellipticals (*triangles*) but extend their range to even lower masses and higher surface brightnesses. This continuity in structure is consistent with the continuity in rotation, disk, and radio properties noted above. It also strengthens the notion that bulges and intermediate ellipticals intrinsically belong to one smooth, unbroken sequence. In this view, bulges are those hot stellar systems that formed from either the highest density and/or most dissipative initial conditions. From the discussion above, we further expect that the formation of bulges involved mergers that contained the highest fraction of gas. Although the M/L of bulges is somewhat offset from the fundamental plane (§ 4.1), there appear to be several natural explanations for this, and it is probable that this difference is fairly superficial, rather than reflecting any fundamental distinction between bulges and ellipticals. We conclude that bulges are simply an extension of the natural GS continuum to even smaller masses.

4.4. *The Distribution of Compact Ellipticals within the Fundamental Plane*

Compact galaxies are shown as cirles in Figures 2 and 4. The three relatively nearby prototype compact elliptical galaxies, NGC 4486B, NGC 5846A, and M 32 (King 1962; Faber 1973; Nieto & Prugniel 1987), pose somewhat of a challenge for morphological classification, as these three galaxies are clearly much more compact than other nearby ellipticals. Prugniel (1989) has analyzed other candidates for compact ellipticals (mainly from Binggeli, Sandage, & Tammann 1985), but finds that when investigated in detail, no other ellipticals are as compact as these three galaxies. Indeed, of the over 350 galaxies combined between our sample and that of the seven Samurai (Faber et al. 1989), only the most extreme bulges (NGC 4026, NGC 4111, NGC 7332) and one other elliptical (NGC 5845) are as compact as the three prototypes.

Five other galaxies in our sample have been morphologically classified as compact at some time—IC 767, NGC 2694, NGC 3641, NGC 4467, and VCC 351. None of these are in fact very compact, although IC 767 seems to share the common property with M 32 of having a low central velocity dispersion. On this slim basis we provisionally place IC 767 among the compact ellipticals and classify the other four galaxies as low or intermediate luminosity ellipticals. The conclusions below do not depend strongly on this choice.

The two rotationally flattened *bona fide* compacts, NGC 4486B and NGC 5846A, follow closely the relationship defined by the bulges. This gives added credence to the reality of the bulge-intermediate elliptical sequence and serves further to identify such compacts as similar to the bulges of disk galaxies.

The best examples of compact galaxies are found in the close vicinity of much more luminous galaxies. The high degree of similarity the physical properties of bulges and rotationally supported compacts suggests a common formation mechanism. In this view, rotationally supported compacts are bulges that did not manage to acquire a disk due to their proximity to the much stronger gravitational field of a massive neighbor (a similar point of view has been discussed by Nieto 1990 and Davidge 1991). The rarity of such galaxies would suggest that this does not often happen during galaxy formation.

The anisotropic compact M32 lies well away from the bulges and the other compacts in a position that defines easy explanation. Like the other compacts, it lies close to a much bigger galaxy, yet it is *an*isotropic and has exceptionally low mass. It is clearly a special galaxy in our sample, although IC 767 shares its anisotropy. Perhaps the uniqueness of M32 is indeed due to some extra tidal stripping (King 1962; Faber 1973; Nieto & Prugniel 1987). Whether this could also explain its anisotropy is unclear.

4.5. *The Distribution of Dwarf Hot Galaxies within the Fundamental Plane*

The above discussion has identified three types of hot galaxies—bulges, compacts, and luminous ellipticals—and grouped them in a single family under the GS continuum hypothesis. We now turn to dwarf hot galaxies, which appear to constitute a totally separate group (cf. Kormendy 1985, 1987).

Although the bright dwarf ellipticals (*diamonds*) define a plane that parallels the main fundamental plane with a small offset in κ_3, their distribution *within* that plane is very different from the plane defined by the luminous elliptical/bulge

sequence. As is well known, the bright dwarf ellipticals follow different scaling relations from those of luminous galaxies and bulges. The surface brightnesses of dwarf ellipticals increase with luminosity (e.g., Kormendy 1985; Binggeli et al. 1985); in our coordinates, κ_2 increases with κ_1. The longest axis of the distribution of bright dwarf ellipticals is *perpendicular* to the relationship defined by luminous ellipticals and bulges. The dwarf spheroidals (*small squares*) appear to form an extension to the bright dwarfs as viewed in projection onto the plane but lie above the plane when viewed edge on (§ 4.1).

4.5.1. *The Origin of Dwarf Hot Galaxies*

It has been suspected for a long time (Larson 1974; Saito 1979a,b; Dekel & Silk 1986; Vader 1986; Yoshii & Arimoto 1987) that significant wind-driven mass loss may differentiate dwarf ellipticals from more luminous hot stellar systems (see the process vectors in Fig. 2*b*), Dekel & Silk (1986), as well as Schaeffer & Silk (1988), concluded that winds should start to become important below a certain velocity dispersion threshold, which they expected to lie between 60 km s^{-1} and 120 km s^{-1}.

The locus of bright dwarf ellipicals intersects the sequence of luminous ellipticals and bulges at $\kappa_1 \approx 3$ and $\kappa_2 \approx 3.5$, corresponding to roughly $\sigma_0 = 100$ km s^{-1}, $r_e = 1$ kpc, and $SB_e = 21$ mag arcsec^{-2}. This value of σ_0 is consistent with the wind prediction. Indeed, the bright dwarfs are more clearly distinguished from luminous ellipticals and bulges by σ_0 than by any other parameter (Fig. 2*b*).

At first glance, the bright dwarfs appear to populate a one-dimensional sequence in the fundamental plane, terminated at one extreme by the dwarf spheroidals. It is tempting to identify this sequence with progressively larger amounts of mass loss, starting with a single progenitor galaxy type near $\kappa_1 \approx 3.5$, $\kappa_2 \approx 4.0$. This is *not* an admissible interpretation, however, because the vector direction for mass loss does not parallel the dwarf locus. The mass-loss vector is much steeper, owing to the fact that I_e^3 is reduced proportionally much faster than mass. Relinquishing adiabaticity would likely cause I_e to decline even faster.

Thus, if dwarf ellipticals are indeed produced by mass loss (and we give below some evidence that they are), they could not have come from a common progenitor but rather must have come from a *range* of progenitors lying at lower values of κ_1 in the fundamental plane than luminous ellipticals and bulges. These progenitors are not represented in our diagrams and are therefore not among the hot stellar systems of today. Perhaps these progenitors no longer exist. Or, perhaps some avoided mass loss and evolved to become low-luminosity spirals and/or irregulars. Identifying these progenitors, if they exist today, may be possible once means are developed to plot other Hubble types in κ-space.

For now, the dwarf "sequence" presents something of a puzzle. Why, with a range of possible progenitors and variable amounts of mass loss, would dwarf ellipticals now populate a *one*-dimensional sequence rather than a two-dimensional sheet? The answer may lie at least partly in two important selection effects: (i) Galaxies that would naturally lie above the dwarf sequence (at higher κ_3) would have experienced less mass loss and may be higher surface brightness systems that are more disklike and, hence, not included in our sample. It is unlikely that such galaxies are simply undiscovered *hot* stellar systems, as such galaxies should be easy to detect (e.g., by Binggeli et al. 1985). (ii) Galaxies that lie below the sequence may have surface brightnesses too low to permit either detection or, if detected, accurate determination of velocity dispersion. Until such selection effects are understood, interpretation of the dwarf "sequence" remains uncertain.

A second scenario for the formation of dwarf ellipticals involves ram-pressure stripping from gas-rich irregulars and small spirals. This could happen within clusters or in the vicinity of a more luminous companion (for instance, the Local Group dwarf spheroidals may have lost their gas in interaction with the Galaxy; Faber & Lin 1983). The predictions of this picture for our purposes are similar in every way to those of wind-driven mass loss.

A third scenario for the formation of dwarfs is that they may be tidal debris left over from the merging of more luminous galaxies (Gerola, Seiden, & Schulmann 1980; Gerola, Carnevali, & Salpeter 1983). Although this alternative seems unlikely due to considerations of mass and angular momentum (see below), computer modeling is needed to explore this scenario fully. It should also be noted that winds would likely operate at some level for the second and third scenarios.

4.5.2. *A Possible Origin of Anistropy in Dwarf Ellipticals*

Ironically, those galaxies that define the extrema of the properties of hot stellar systems—dwarf ellipticals and giant ellipticals—are both supported by anisotropic velocity dispersions (filled symbols in Fig. 2). These galaxies are separated in mass by a small strip of rotationally flattened galaxies. This is the first hint that anisotropy in dwarfs may have a different origin than in giant ellipticals.

While the merger hypothesis is the most promising explanation for the anisotropy of luminous ellipticals, this possibility seems rather unlikely for the dwarfs. This point of view is supported by the observation that anisotropic dwarf ellipticals, compact ellipticals, and rotationally flattened luminous ellipticals *together* seem to follow a *single* relation between specific angular momentum and luminosity (J/M; BN90). In contrast, luminous *anisotropic* ellipticals have systematically lower specific angular momenta than this relation predicts. Therefore, anisotropies in luminous and dwarf ellipticals are most likely of different origin.

As has been discussed by BN90, reexpansion after mass loss (either by a supernova-driven wind or by ram-pressure stripping) may account for the anisotropic velocity dispersions of dwarf ellipticals. Alternately, the protosystems from which dwarf ellipticals formed might not have isotropized their velocity dispersions due to very low initial density and, in consequence, a low collision rate within the molecular cloud system (Bender et al. 1991).

5. DISCUSSION AND QUESTIONS

This paper has compared the structural properties of ellipticals, bulges, compact ellipticals, and dwarf ellipticals as described in the 3-space defined by the global parameters σ_0, SB_e, and r_e. We find that all types of hot stellar systems, except the very low luminosity dwarf spheroidals, define planes in this space with possible small, parallel offsets between classes. This observation is consistent with virial equilibrium, coupled with the assumption that the structural properties and mass-to-light ratios change only a little as a function of the three basic parameters, independent of the type of hot stellar system studied. The lowest luminosity dwarf spheroidals are distributed perpendicular to the fundamental plane, owing to the higher mass-to-light ratios of these dark-matter–dominated,

faint galaxies. We can rephrase these thoughts as follows: *The structural parameters of all baryon-dominated hot stellar systems are confined close to the fundamental plane.*

Various types of hot stellar systems populate systematically different regions within the fundamental plane. One overlapping family of luminous systems can be identified, comprised of various subgroups. The less luminous half of this family is composed of systems that are mostly rotationally flattened, including intermediate ellipticals, bulges, and compact ellipticals. The brighter portion of this family contains primarily anisotropic giant ellipticals. Structural data, combined with other kinds of morphological data (Table 1) suggest that rotationally flattened ellipticals are similar to S0's in which the disk is too faint to be easily recognized. Likewise, compact ellipticals may be the bulges of failed disk galaxies that could not acquire significant disks due to the tidal field of nearby massive galaxies. The possibility that some compact ellipticals are tidally truncated is also consistent with these data.

Taken together, the entire family of ellipticals, bulges, and compacts forms a continuous sequence in which, with increasing mass, galaxies on average become more anisotropic in their velocity distribution, the frequency of faint stellar S0-like disks decreases, the frequency of unrelaxed velocity fields increases, and surface brightness declines. These observations together suggest that the most luminous ellipticals are less dissipated than their fainter counterparts. If all ellipticals had dissipated by similar amounts, surface brightness would hardly change as a function of mass (at least in the CDM picture). The lower dissipation of giant ellipticals is consistent with a GS continuum, in which galaxies formed from progenitors with lower gas-to-star ratios at higher total mass. (This could involve the formation of giant ellipticals out of smaller galaxies, including small ellipticals, but such an evolutionary scenario is not required.)

The other clear group within the fundamental plane is the dwarf galaxies. The longest axis of this sequence is nearly perpendicular to the longest axis of the bulge/elliptical sequence, and surface brightness *increases* with mass. At fixed mass, the surface brightnesses of bright dwarf ellipticals are systematically lower and the M/L ratios slightly higher than those of giant ellipticals, and these differences become much higher for the faintest dwarfs. These effects can be understood via variable amounts of mass loss through either galactic winds or ram-pressure stripping. Although dwarf ellipticals seem to be generally anisotropic systems, their anisotropy likely has a different origin from the anisotropy of luminous ellipticals. It may be that inflation of the dwarf galaxies due to mass loss is the origin of their anisotropy. Another possibility may be that the collapse of dwarfs was not sufficient to isotropically mix the protogalactic mass concentrations.

A general conclusion is that hot stellar systems that are rotationally flattened are on average more significantly concentrated than anisotropic hot stellar systems. The latter galaxies either experienced a violent *dissipationless* merging process (luminous Es) or suffered from significant mass loss (dwarf ellipticals), which caused either an early halt in collapse or perhaps even reexpansion.

Whatever our success in interpreting the structural parameters of hot stellar systems, one result is clear: As we delve further into the details of the physical structure of these systems, we continue to find that these details are at once both more complex, yet simpler, than we once thought. Ellipticals with similar global structural properties posseses a range of internal structural details. Conversely, ellipticals with very different global properties share certain specific internal physical details.

Piecing this puzzle further together requires additional information. One of the main players in this game, the stellar populations of these galaxies, is only superficially represented in the fundamental plane. The relationship of the kinds of stars in hot stellar systems to their parent systems will be the subject of Paper II in this series. If mergers and dissipation play important roles in the formation of hot stellar systems, one will also have to address the relationship of hot stellar systems to cold stellar systems (i.e., disk-dominated galaxies). It is our goal in future papers to develop a suitable formalism for studying such a relationship.

Partial support for this research was provided by NSF grant AST-9016930 and NASA grant NAG 5-547 (D. B.), DGF grant SFB 328 (R. B.), and AST 8702899 (S. M. F.). We thank the anonymous referee for helpful comments.

APPENDIX A

STRUCTURE CONSTANTS FOR KING GALAXY MODELS

Distribution functions developed by King (1966) have been shown to represent well the surface brightness profiles of both dwarf ellipticals (e.g., Binggeli & Cameron 1991) and giant ellipticals (e.g., NGC 4472, King 1966). Ellipticals of intermediate luminosity are less well fitted, due to their relatively small core radii relative to their effective radii (Kormendy 1985). The ratio between tidal radius r_t and core radius r_c (the radius at which the surface brightness has dropped to half its central value) is about 100–300 for giant ellipticals and lies between 5 and 20 in case of dwarfs.

If we assume an isotropic velocity dispersion, the Poisson equation for the King models can readily be integrated (see Binney & Tremaine 1987), and we can establish relations between the major scaling parameters (σ_0, I_e, r_e, M, and L) that can be parametrized by the two structural parameters, c_1 (eq. [2], § 3.1) and c_2 (eq. [3]). If effective surface brightness I_e is simply defined as the mean surface brightness *within* the effective radius, the structural parameter c_1 is identically 2π. [This would not be the case had we used surface brightness at the effective radius. Here I_e measures the surface brightness in $L_\odot$ pc^{-2}, as is related to the definition of SB_e given in Table 1 by $\log I_e = -0.4 \times (SB_e - 27)$.] On the other hand, c_2 depends on r_t/r_c in a nontrivial way due to basic changes in the structure of the galaxy.

We are mainly interested in the ratio c_2/c_1 as a function of r_t/r_c. A series of King models was calculated to explore this relationship, which is plotted in Figure 5. The projected line-of-sight central velocity dispersion was used for σ_0. The ratio c_2/c_1 decreases by about a factor 1.6 from dwarf ellipticals to giant ellipticals in a roughly monotonic fashion. Since a value of c_2/c_1 corresponding to $r_t/r_c \approx 100$ was used for estimating M and M/L in Figures 1–4, masses of dwarf ellipticals are systematically

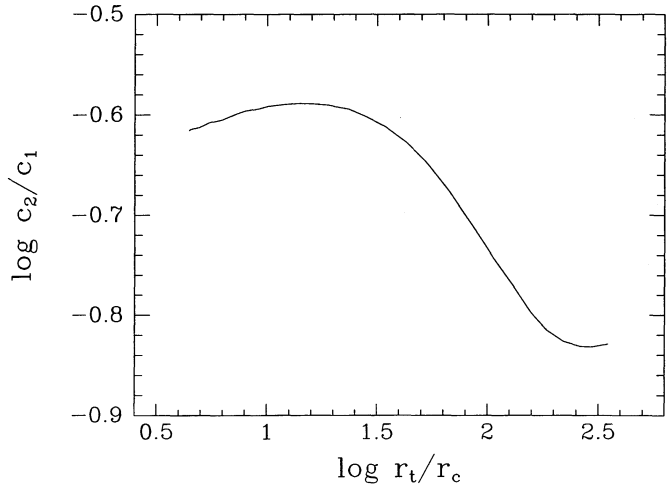

FIG. 5.—The ratio of the structure parameters c_1 and c_2 plotted as a function of the ratio of core radius (r_c) to tidal radius (r_t) for a series of King models

underestimated relative to those of giant ellipticals by about a factor of 1.5. Hence, appealing to changes in c_2 will not explain the higher M/L values of dwarf galaxies.

These considerations do not take into account the influence of different internal kinematics (like different degrees of anisotropy). Estimating these uncertainties is beyond the scope of this paper and is very difficult because even a complete knowledge of the projected velocity field is not sufficient to constrain the kinematic structure sufficiently (e.g., Richstone & Tremaine 1986).

APPENDIX B

EFFECT OF ROTATIONAL SUPPORT ON MASS ESTIMATES

The mass estimates made in the text of the paper take into account only the random kinetic energy and neglect rotational support and flattening. The tensor virial theorem (Binney & Tremaine 1987; BT) can be used to estimate the rotational support correction to these mass estimates. Start with the trace of the tensor virial theorem, $KE = T + \Pi = -W$, where T is the kinetic energy of ordered motion (rotation), Π is the kinetic energy of random motion, and W is potential energy. Estimates are made for each of these terms for an isotropic oblate rotator of mass M, central velocity dispersion σ_o, rotation velocity v, axial ratio a_3/a_1, and ellipticity $\epsilon = 1 - a_3/a_1$.

Let the subscript "o" denote the naive estimate of energies with rotation and flattening neglected; i.e., $KE_o = \Pi_o$. From this, we can write $KE = KE_o(1 + \delta)$, where $\delta \equiv 1/3 \times v/\sigma_o^2$ is just the fractional change in kinetic energy due to rotation. The relationship between v/σ_o and ϵ for oblate rotators is taken from BT and given in Table 3 below.

The effect of flattening on the potential energy W of an oblate spheroid can be estimated as follows. BT give formulae for the potential energies of flattened ellipsoids. There is a correction term that depends only on the flattening, multiplied by a term that depends only on the density distribution. Assume that the density distribution of the oblate rotator is derived from a spherical galaxy simply by contracting the galaxy along the z-axis, accompanied by an overall expansion to maintain constant effective radius. Since our effective radii for flattened ellipticals are closely equal to $(ab)^{1/2}$ (a and b are the usual definition of major and minor axis), the old spherical radii, a_o is related to the new radii via $a_o = (a_1 a_3)^{1/2}$, or $a_o/a_3 = (a_1/a_3)^{1/2}$.

Since the correction term for flattening does not depend on the density distribution $\rho(r)$, it can be obtained from Table 2-2 of BT for homogeneous ellipsoids. For the general case,

$$W = \frac{-8}{15}\,\pi^2 G\rho^2 a_1 a_2 a_3 I a_1^2\,, \tag{8}$$

TABLE 3

CORRECTION FACTORS FOR ENERGIES AND MASSES OF ROTATING OBLATE GALAXIES

ϵ	a_3/a_1	δ	η	$1 + \delta/\eta$
0.0.....	1.0	0.00	1.000	1.00
0.2.....	0.8	0.07	0.959	1.12
0.4.....	0.6	0.21	0.897	1.35
0.5.....	0.5	0.33	0.856	1.55
0.6.....	0.4	0.48	0.800	1.85

where

$$e = \sqrt{1 - (a_3/a_1)^2} \text{ and } I = 2\frac{\sqrt{1-e^2}}{e} \arcsin e \, .$$

For a uniform sphere, this resolves to

$$W_o = \frac{-16}{15} \pi^2 G \rho_o^2 a_o^2 \, . \tag{9}$$

For an oblate spheroid, W is given by eqn. (8) with a_2 set equal to a_1. Thus, the correction to potential energy for flattening, η, is

$$\eta = W/W_o = \frac{a_1^4 a_3}{a_o^5} \left(\frac{\rho}{\rho_o}\right)^2 \frac{\sqrt{1-e^2}}{e} \arcsin e \, . \tag{10}$$

The requirement that mass is conserved implies $\rho/\rho_o = a_o^3/a_1^2 a_3$. Thus,

$$\eta = \frac{a_o}{a_3} \frac{\sqrt{1-e^2}}{e} \arcsin e = \sqrt{\frac{a_1}{a_2}} \frac{\sqrt{1-e^2}}{e} \arcsin e \, ,$$

using the relationship among a_o, a_1, and a_3 defined above.

The corrected virial theorem for the oblate rotator is $(1 + \delta)KE_o = \eta W_o$, resulting in $M = (1 + \delta)/\eta \, M_o$, where M_o is the naive mass without taking into account rotation and flattening and $(1 + \delta)/\eta$ is the correction term for rotation and flattening.

This correction is listed in Table 3 for various values of the ellipticity. Neglect of rotation and flattening leads to a significant underestimate of M and M/L for rapidly rotating spheroidal galaxies. According to BT, the maximum ellipticity of rotating ellipticals is ~ 0.4, for which the mass correction is 1.35, or 0.13 dex. Rotating bulges approach ellipticities of 0.55, for which the correction is ~ 1.7, or 0.23 dex.

In evaluating whether these factors can have an appreciable impact on the κ_3 residuals of rotating galaxies in Figure 3, the effects on both κ_1 and κ_3 must be taken into account. One finds that $\delta\kappa_3 = -0.47\Delta \log M$ if L is held constant. If the average ellipticity of bulges is half the maximum value of 0.55, the average offset in κ_3 would be -0.06, which is about one-half the median amount observed. Thus, a rotational correction to the mass estimate for bulges is significant, but cannot completely explain the offset of bulges in Figure 3. In this context, we note that, if L differs at a given M for reasons not related to dynamics (e.g., different mean ages of the stars in galaxies), M is held constant, and $\delta\kappa_3 = -0.58\Delta \log M/L$. Finally, the somewhat smaller net offset of $\delta\kappa_3$ for rotating ellipticals is consistent with an average correction of ~ 0.06 dex to their masses for rotational support, as implied by their ellipticities.

REFERENCES

Aaronson, M. 1983, ApJ, 266, L11
Barnes, J. E. 1988, ApJ, 331, 699
Barnes, J., & Hernquist, L. 1991, ApJ, 370, L65
Bender, R. 1988a, A&A, 193, L7
———. 1988b, A&A, 202, L5
———. 1990, in Dynamics and Interactions of Galaxies, ed. R. Wielen (Heidelberg: Springer), 232
———. 1991, in Morphological and Physical Classification of Galaxies, ed. Busarello et al. (Dordrecht: Kluwer), in press
———. 1992, in IAU Symp. 149, The Stellar Populations of Galaxies, ed. B. Barbuy (Dordrecht: Kluwer), in press
Bender, R., & Nieto, J.-L. 1990, A&A, 239, 79 (BN90)
Bender, R., Paquet, A., & Nieto, J.-L. 1991, A&A, 246, 349
Bender, R., Surma, P., Döbereiner, S., Möllenhoff, C., & Madejsky, R. 1989, A&A, 217, 35
Bertola, F., Burstein, D., & Buson, L. M. 1993a, ApJ, in press
Bertola, F., Burstein, D., Buson, L. M., & Renzini, A. 1993b, ApJ, in press
Binggeli, B., & Cameron, L. M. 1991, A&A, 252, 27
Binggeli, B., Sandage, A., & Tammann, G. A. 1985, AJ, 90, 1681
Binney, J., & Tremaine, S. 1987, Galactic Dynamics (Princeton: Princeton Univ. Press) (BT)
Blumenthal, G. R., Faber, S. M., Primack, J. R., & Rees, M. J. 1984, Nature, 311, 517
Brocato, E., Matteucci, F., Mazzitelli, I., & Tornambé, A. 1990, ApJ, 349, 458
Burstein, D. 1978, Ph.D. thesis, University of California, Santa Cruz
———. 1990, Rep. Prog. Phys., 53, 421
Burstein, D., & Heiles, C. 1984, ApJS, 54, 33
Burstein, D., Bertola, F., Buson, L. M., Faber, S. M., & Lauer T. R. 1988a, ApJ, 328, 440
Burstein, D., Davies, R. L., Dressler, A., Faber, S. M., Lynden-Bell, D., Terlevich, R., & Wegner, G. 1987, ApJS, 64, 601
———. 1988b, in Towards Understanding Galaxies at Large Redshift, ed. R. G. Kron & A. Renzini (Dordrecht: Kluwer), 17
Davidge, T. J. 1991, AJ, 102, 896
Davies, R. L., & Birkinshaw, M. 1988, ApJS 68, 409
Davies, R. L., Burstein, D., Dressler, A., Faber, S. M., Lynden-Bell, D., Terlevich, R. J., & Wegner, G. 1987, ApJS, 64, 581
Davies, R. L., & Illingworth, G. D. 1983, ApJ, 266, 516
Davies, R. L., Efstathiou, G., Fall, S. M., Illingworth, G. D., & Schechter, P. 1983, ApJ, 266, 41 (DEFIS)
Dekel, A., & Silk, J. 1986, ApJ, 303, 39
de Vaucouleurs, G., de Vaucouleurs, A., & Corwin, H. G., Jr. 1976, Second Reference Catalog of Bright Galaxies (Austin: Univ. Texas Press)
Djorgovski, S., & Davis, M. 1987, ApJ, 313, 59
Dressler, A., Lynden-Bell, D., Burstein, D., Davies, R. L., Faber, S. M., Terlevich, R. J., & Wegner, G. 1987, ApJ, 313, 42
Faber, S. M. 1973, ApJ, 179, 423
———. 1982, in Astrophysical Cosmology, ed. H. Brück et al. (Vatican: Pontificia Academia Scientiarum), 191
———. 1984, in Large-Scale Structure of the Universe, Cosmology and Fundamental Physics (First ESO-CERN Symposium), ed. G. Setti, & L. Van Huve (ESO: Garching), 187
———. 1992, in IAU Symp. 149, The Stellar Populations of Galaxies, ed. B. Barbuy (Dordrecht: Kluwer), in press
Faber, S. M., & Burstein, D. 1988, in Large-Scale Motions in the Universe, ed. V. C. Rubin, & G. V. Coyne, S. J., (Princeton: Princeton Univ. Press), 115
Faber, S. M., Dressler, A., Davies, R. L., Burstein, D., Lynden-Bell, D., Terlevich, R., & Wegner, G. 1987, in Nearly Normal Galaxies, From the Planck Time to the Present, ed. S. M. Faber (NY: Springer), 175
Faber, S., & Lin, D. 1983, ApJ, 266, L17
Faber, S. M., Wegner, G., Burstein, D., Davies, R. L., Dressler, A., Lynden-Bell, D., & Terlevich, R. J. 1989, ApJS, 69, 763
Franx, M., & Illingworth, G. 1988, ApJ, 327, L55
Franx, M., Illingworth, G., & Heckman, T. M. 1989, ApJ, 344, 613
Freeman, K. C. 1987, in Nearly Normal Galaxies, From the Planck Time to the Present, ed. S. M. Faber (New York: Springer), 317
Gerola, H., Carnevali, P., & Salpeter, A. A. 1983, ApJ, 268, L75
Gerola, H., Seiden, P., & Schulmann, L. 1980, ApJ, 242, 517
Gott, J. R., & Rees, M. J. 1975, A&A, 45, 465
Gregg, M. G. 1989, ApJ, 337, 45
Gunn, J. E. 1987, in Nearly Normal Galaxies, From the Planck Time to the Present, ed. S. M. Faber (New York: Springer), 455
Hernquist, L., & Barnes, J. E. 1991, Nature, 354, 210
Hills, J. G. 1980, ApJ, 225, 986

Jedrzejewski, R. I., & Schechter, P. L. 1988, ApJ, 330, L87
Kent, S. M. 1985, ApJS, 59, 115
———. 1987, AJ, 94, 306
King, I. R. 1962, AJ, 67, 471
———. 1966, AJ, 71, 64
Kormendy, J. 1985, ApJ, 295, 73
———. 1987, in Nearly Normal Galaxies, From the Planck Time to the Present, ed. S. M. Faber (New York: Springer), 163
———. 1989, ApJ, 342, L63
———. 1990, in Dynamics and Interactions of Galaxies, ed. R. Wielen (NY: Springer), 499
Kormendy, J., & Illingworth, G. 1982, ApJ, 256, 460
Larson, R. B. 1974, MNRAS, 169, 229
Lauer, T. R. 1985, ApJ, 292, 104
Lucey, J. R., Bower, R. G., & Ellis, R. S. 1991, MNRAS, 349, 755
Mateo, M., Olszewski, E., Welch, D. L., Fischer, P., & Kunkel, W. 1991, AJ, 102, 914
Nieto, J.-L. 1988, Bol Acad Nac Cien Cordoba, 58, 239
———. 1990, in Dynamics and Interactions of Galaxies, ed. R. Wielen (NY: Springer), 258
Nieto, J.-L., & Prugniel, P. 1987, in IAU Symp. 127, Structure and Dynamics of Elliptical Galaxies, ed. T. de Zeeuw (Dordrecht: Reidel), 99
Ostriker, J. P. 1980, Comm. Ap., 8, 177
Paltoglou, G., & Freeman, K. C. 1987, in IAU Symp. 127, Structure and Dynamics of Elliptical Galaxies, ed. T. de Zeeuw (Dordrecht: Reidel), 447
Prugniel, P. 1989, Ph.D. thesis, Université Paul Sabatier, Toulouse
Richstone, D., & Tremaine, S. 1986, AJ, 92, 72
Rix, H.-W., & White, S. D. M. 1990, ApJ, 362, 52
Saito, M. 1979a, PASJ, 31, 181
———. 1979b, PASJ, 31, 193
Sandage, A., Binggeli, B., & Tammann, G. A. 1985, in The Virgo Cluster, (Proc. ESO Conf. No. 20) ed. O.-G. Richter & B. Binggeli (Garching: ESO), 239
Sandage, A., & Trammann, G. A. 1981, A Revised Shapley-Ames Catalog of Bright Galaxies (Washington: Carnegie Institution)
Sandage, A., & Visvanathan, N. 1978, ApJ, 223, 707
Schaeffer, R., & Silk, J. 1988, A&A, 203, 273
Schechter, P. L., & Gunn, J. E. 1979, ApJ, 229, 472
Schweizer, F. 1982, ApJ, 252, 455
———. 1990, in Dynamics and Interactions of Galaxies, ed. R. Wielen (NY: Springer), 60
Schweizer, F., Seitzer, P., Faber, S. M., Burstein, D., Dalle Ore, C. M., & Gonzalez, J. J. 1990, ApJ, 364, L33
Seifert, W. 1990, Ph.D. thesis, University of Heidelberg
Silk, J. R. 1983, Nature, 301, 574
Sulentic, J. W., & Tifft, W. G. 1974, The Revised General Catalogue of Non-stellar Astronomical Objects (Tucson: Univ. Arizona Press)
Tonry, J. L. 1984, ApJ, 283, L27
Toomre, A. 1977, in The Evolution of Galaxies and Stellar Populations, ed. B. M. Tinsley & R. B. Larson (New Haven: Yale Univ. Obs), 401
Vader, J. P. 1986, ApJ, 305, 669
White, S. D. M., & Rees, M. 1978, MNRAS, 183, 341
Whitmore, B. C., McElroy, D. B., & Tonry, J. L. 1985, ApJS, 59, 1
Yahil, A., Tammann, G. A., & Sandage, A. 1977, ApJ, 217, 903
Yoshii, Y., & Arimoto, N. 1987, A&A, 188, 13
Zinn, R. 1985, Mem. Soc. Astron. Ital., 56, 223